ISRU Pilot Excavator (IPEx) Technology Readiness Level 5 Design Overview

Jason M. Schuler[1], Jonathan D. Smith[2], Andrew J. Nick[3], Bradley C. Buckles[4], Jeffrey E. Dyas[5], Victoria V. Ortega[6], Joseph M. Cloud[7], Adam G. Dokos[8], Elizabeth L. Zhang[9], Jerry J. Wang[10], Michael A. Baron[11]

National Aeronautics and Space Administration, Kennedy Space Center, Florida, 32899, U.S.A

Thomas J. Muller[12]

Bennett Aerospace, Glenwood Ave, North Carolina, 27603, U.S.A

Casey J. Clark[13]

Astrion, Washington, DC, 20024, U.S.A

Musashi W. Howe[14]

Aetos Systems, Huntsville, Alabama, 35806, U.S.A.

This paper details the mechanical and mechatronic design of the Technology Readiness Level (TRL)-5 In-Situ Resource Utilization (ISRU) Pilot Excavator (IPEx). IPEx is a robotic excavator designed for a technology demonstration of regolith mining in the lunar south pole region. The novel design uses pairs of counter-acting excavation tools called bucket drums, that dig at the same time in opposing directions to reduce the reaction force needed, thereby enabling mining with a small, low-mass, robotic system. IPEx builds on the prior work of the Regolith Advanced Surface Systems Operations Robot (RASSOR), which is the TRL-4 implementation of this concept. The TRL-5 IPEx subsystems that are discussed in this paper include: Regolith Delivery Subsystem (RDS), Mobility Subsystem (MS), Cameras and Dust Mitigation Subsystem (CDMS), and Thermal Control Subsystem (TCS). Each subsystem is described in detail with rationale for design selections. Dust tolerance is a key feature for IPEx, and this paper details a thermal control system with an actuated radiator cover and phase change material as well as camera modules with removable electrodynamic dust shields (EDS). Additional components such as actuators, wheels, and bucket drums are discussed in detail. Due to their complexity, the avionics and software subsystems will be discussed in a separate publication.

---

[1] IPEx Principal Investigator, Kennedy Space Center.
[2] IPEx Lead Mechanical Engineer, Kennedy Space Center.
[3] IPEx Lead Controls Engineer, Kennedy Space Center.
[4] IPEx Lead Software Engineer, Kennedy Space Center.
[5] IPEx Lead Systems Engineer, Kennedy Space Center.
[6] Mechanical Engineer, Kennedy Space Center.
[7] Robotics Engineering Trainee, Kennedy Space Center, AIAA Student Member.
[8] Mechanical Engineer, Kennedy Space Center.
[9] Mechanical Engineering Trainee, Kennedy Space Center.
[10] Electrostatics Researcher, Kennedy Space Center.
[11] Mechanical Engineer, Kennedy Space Center.
[12] Research & Development Engineer, Kennedy Space Center.
[13] Research & Development Engineer, Kennedy Space Center.
[14] Research & Development Engineer, Kennedy Space Center.

I. Introduction

NASA's goal of sustainable exploration of the Moon and Mars will be enabled by utilizing locally sourced resources such as oxygen. This approach will reduce the supplies launched from Earth and is known as In-Situ Resource Utilization (ISRU) [1]. Many of the resources available on the Moon can be found in the outer layer of loose rocky material known as regolith. The regolith can be excavated and processed to extract the desired elements and can also be used directly as a construction material.

To date, NASA missions have only excavated tens of kilograms of lunar regolith [2]. Excavation has never been performed by a dedicated excavation technology/robot, rather only as a secondary function of an exploration rover or by an astronaut using scooping/sampling methods. The ISRU Pilot Excavator (IPEx) will be NASA's first lunar surface robot specifically designed with the reliability and efficiency to excavate large quantities of regolith. This capability is critical to sustained lunar mission success. By the start of the next decade, the excavation needs will increase from sampling levels to tens or hundreds of tons of regolith per year [3]. Going beyond this to full-scale sustained ISRU and construction of infrastructure will increase that amount to thousands of tons of regolith per year.

The IPEx project is developing a 30 kg-class excavator to demonstrate robotic excavation of large amounts (10,000 kg) of granular lunar regolith on a future technology demonstration mission. IPEx uses novel excavation tools, called bucket drums, which are hollow cylinders with scoops staggered around the outside. Regolith is collected with the scoops and flows into the drum where it is captured by an internal baffle system. The excavator can then transport the regolith in the drum and reverse the direction of the drum rotation to dispense the regolith back out. IPEx uses two sets of bucket drums that dig simultaneously in opposing directions and results in counter-acting excavation forces. This combination of bucket drum excavation tools and counter-acting excavation forces enables low mass robotic excavators to effectively dig in reduced gravity environments. This is a significant departure from terrestrial excavators that rely on high mass to produce tractive forces to counteract the forces of excavation.

IPEx is targeting excavation of 10,000 kg of granular lunar regolith as a demonstration of the capability that will be needed for a follow-on ISRU demonstration mission referred to as the "ISRU Pilot Plant". For the ISRU Pilot Plant to demonstrate extraction of 1,000 kg of oxygen, 10,000 kg of lunar regolith must be supplied to the ISRU system.

To supply an ISRU Pilot Plant with regolith material the excavator will need to drive further, repeatedly traverse, and excavate more regolith than any other planetary robot to-date. IPEx is being built to a Technology Readiness Level (TRL) 6 "flight-ready" state that is qualified for a notional technology demonstration mission (currently unmanifested). This notional mission would have IPEx prove the advancement in state-of-the-art (SOA) for off-Earth excavation technology by excavating up to 10,000 kg of regolith, at a rate of 42 kg/hr, and covering a total distance of 70 km while operating in the South Pole region of the Moon over 11 days.

The first phase of this development effort involves increasing the TRL from a 4 (as seen in the RASSOR 2 bread board [4]) to a 5 per SP-20205003605, Technology Readiness Assessment Best Practices Guide [5]. To do this, IPEx was decomposed into specific subsystems. Some of these subsystems, from a TRL perspective, are either engineering efforts (e.g. the majority of the Avionics, Ground Software, Deployment), are beyond a TRL-5, or the development is outside the primary goal of the IPEx excavation technology development (e.g. Autonomy/Flight Software). Therefore, those subsystems will not be covered in this publication and do not directly contribute to raising the TRL level of the IPEx subsystems. Furthermore, the subsystems themselves include supporting components to the subsystem's critical assemblies that fall under standard engineering development; focus is strictly on the critical assemblies that are necessary to raise the TRL of the subsystem. With that scope in place, Table 1 below lists the subsystems and their description. Each subsystem is detailed in this paper and the critical assemblies of the subsystem are discussed.

Table 1 IPEx TRL-5 subsystems and descriptions.

Subsystem	Description
Camera and Dust Mitigation System	Encompasses the hardware (cameras, lenses, harnesses, and lighting) to perform visual odometry and localization to enable supervised autonomous navigation along with dust mitigations for this hardware (electro-dynamic dust shields (EDS), camera covers, and hold-down release mechanisms (HDRMs)). It will also be used to establish bearing of the environment during the mission.
Mobility System	The Mobility System is used to support the other subsystems and provide the hardware to drive on the lunar surface. The main hardware components include the structure, wheels, and wheel actuators.

Subsystem	Description
Regolith Delivery System	The Regolith Delivery System (RDS) is used to collect regolith from the lunar surface. It consists of counter-rotating bucket drums on each side of the excavator that are lifted by arms to collect and move lunar regolith. There are actuators for the bucket drums and for the arms. Hardware components include the bucket drums, arms, arm actuators, and bucket drum actuators.
Thermal Control System	The Thermal Control System (TCS) is used to maintain operational temperature ranges for IPEx through transit and a lunar day. Main hardware components consist of a radiator, radiator cover and actuator, phase change material (PCM), heat spreader, heater strips, avionics enclosure, and multi-layer insulation (MLI).

The goals of each of the subsystems are described below in Table 2. These goals are the expectations needed to raise the TRL of each respective subsystem to level 5.

Table 2 IPEx TRL-5 test goals.

Components	TRL-5 Test Goals
Actuator (Wheel, Bucket Drum, Arm, Radiator Cover) Testing	Establish actuator life expectancy for an 11-day mission. Emulate Thermal Mission Profile to perform complete Day-in-the-life testing for each actuator.
Camera and Dust Mitigation System Testing	Validate design can withstand external and internally induced loads. Validate HDRM release. Validate EDS functionality over an 11-day mission.
Wheel and Bucket Drum Parameter Testing	Down-select wheel design via parameter testing (wheel slippage, motor current) and validate fatigue of down-selected wheel in a 11-day mission. Down-select bucket drum material, manufacturing process, and geometry via parameter testing (regolith flow rate, motor current) and validate fatigue of drum in a 11-day mission.

As of June 2024, approximately 95% of the TRL-5 version of IPEx has been designed and 90% fabricated (see Fig. 1).

Fig. 1 IPEx TRL-5 CAD model and build as of January 2024.

II. Actuator Design Philosophy

To reduce schedule and budget, the actuators were designed with as many common parts as possible. Key requirements included mass and volume, but a driver in each of the designs was to build IPEx capable of operating on Earth for testing with the same hardware that will perform the lunar mission. This inherently drove up the torque requirements, resulting in increased size and mass of the actuators, but reduced project complexity by eliminating development of additional weight-accurate versions of IPEx and increased the safety margin for lunar operations. Considering these factors, a frameless kit motor and harmonic drive gear component set were selected for their flexibility and high power-to-weight ratio. After extensive research was conducted to choose an appropriate motor vendor, ThinGap motor company's LS line of frameless motor kits was chosen for meeting power and mass

requirements, as well as having thermal operational ranges suitable for the mission environment. The ThinGap motor company also accommodated custom commutation and motor feedback requirements.

Motor sizing and torque/speed requirements were derived from the mission's concept of operations (ConOps) and a scaling factor was used based off a previous proof of concept excavation robot, RASSOR 2. RASSOR 2 is a fully functioning robotic excavator that is instrumented to gather data such as current draw on the battery and each actuator. By recreating the ConOps for IPEx with RASSOR 2 and recording the current draws, the team was able to estimate the loads imparted on the system. A 1-dimensional scaling factor of approximately 0.7 was used to estimate the physical size of IPEx from RASSOR 2. Recorded currents from RASSOR 2 for each ConOps step were used to back calculated the imparted forces. Those forces were then run through the appropriate equations with the mass, speed, and physical sizes of IPEx to estimate power draw.

A. Actuator Prototype

An initial prototype was designed with the ThinGap motor, harmonic drive, SKF angular contact bearings, hall effect sensors and a resolver for speed and position feedback (see Fig. 2). This actuator was designed, fabricated, and assembled to be tested as a complete actuator unit or as individual components. For this Generation 1 prototype, the team sought to individually test the motors separately from the gearboxes. This approach enabled the characterization of input and output bearings, motor-only performance, gearbox-only performance, seal drag, and a Hall sensor-only option versus a Hall and resolver sensor option.

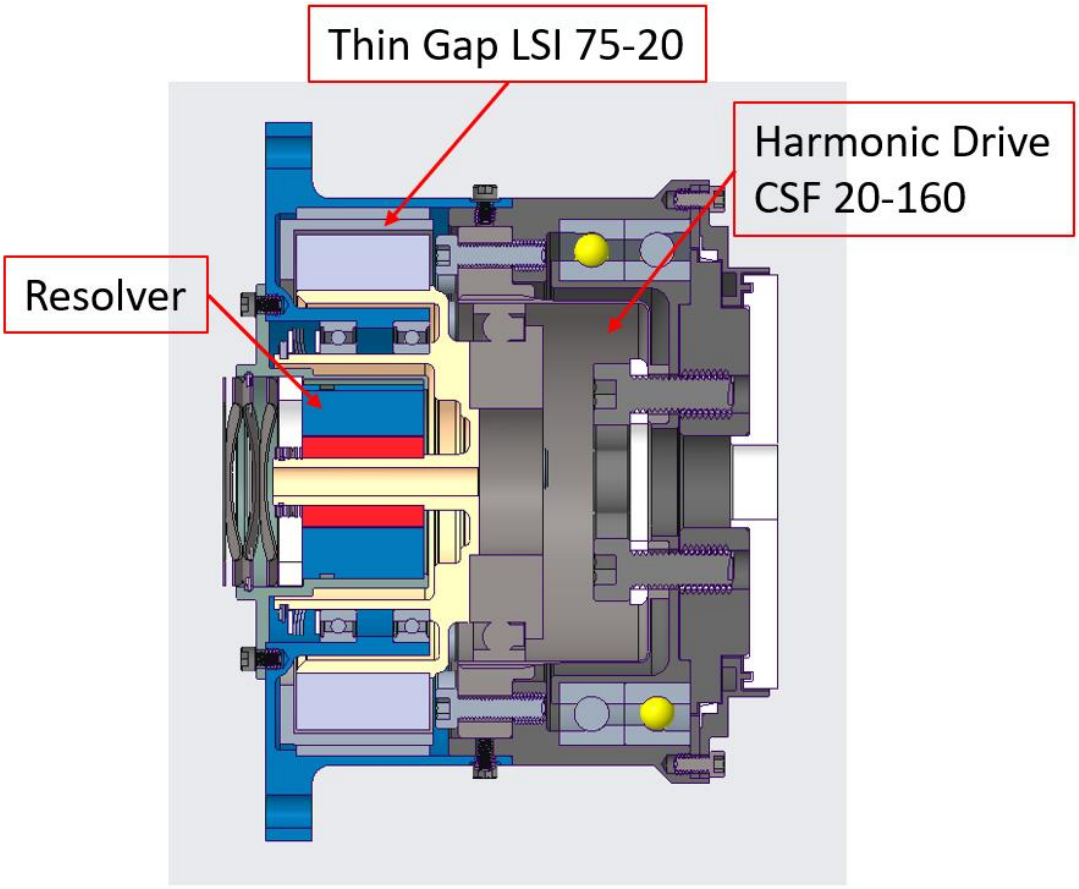

Fig. 2 IPEx Generation 1 prototype actuator.

Motor speeds as low as 25 RPM were required during portions of the ConOps, such as docking to the wireless charger at the lander for the wheel actuators and for arm movements. The resolver was initially intended for speed control at lower velocities due to the direct drive nature of the motor and for providing absolute position feedback.

During the setup and tuning of this Generation 1 prototype actuator, it was noted that the resolver produced significant electrical noise, causing the motor controller to react erratically. Further testing in a Hall sensor-only configuration determined that the resolver was unnecessary for speed control, as the Hall sensors combined with the high pole count of the ThinGap motors effectively met the low velocity requirements. It was concluded that the resolver was not needed for any of the actuators due to the added complexity, mass, volume, and wiring it entailed. Although removing the resolver resulted in the loss of absolute positioning after power cycles, which would have been used for the arm actuator, this issue was mitigated by implementing a homing routine and a strategy for continually saving the current arm position in software.

B. Actuator Test Campaign

Actuator Testing (which includes the wheel, arm, and bucket drum actuators) consists of four unique tests. Each actuator will be configured separately in performing these. Each actuator will be exposed to vacuum for all tests, and dirty vacuum for the ConOps test. TC1 through TC4 encompass the Kennedy Space Center (KSC) Actuator Qualification Test campaign.

TC1 - Motor Characterization Testing: Define torque curves at no load and at incrementally increasing load cases up to expected max load at nominal temperature. These will be placed in a database to use to support optimization of the next version of each respective actuator. This test will serve to verify nominal operations of a newly assembled actuator for final integration.

TC2 - TVAC Operational Testing: Test the actuators at high- and low-end operational temperature. Two cycles with 4-hour dwells after temperature stabilization. After dwell time, collect motor characterization data at temperature extremes. After completion of TVAC testing, re-perform a tailored motor characterization test at nominal temperature to see deltas. This test can be done following TC1 with the same test configuration. After finishing this test, take actuators out of chamber and disassemble to look for visual deltas to the assembly prior to testing.

The data acquired from the TC1 and TC2 tests are used to empirically derive a unique equation for each motor that calculates the motor output torque in real-time based upon telemetry data (motor temperature, velocity, and active current).

TC3 - Accelerated Life testing: Perform usage rate accelerated life testing for the bucket drum and arm actuators, which entails running each actuator continuously at 2-sigma loads (68% of max expected mission load) at the max expected mission temperature and providing the minimum input voltage until it fails or 2x ConOps total revolutions is reached. The wheel actuators were tested in a similar manner by providing minimum input voltage, running at max expected mission temperature at 3-sigma loads (99.7% of max expected mission load) until it fails or 2x ConOps total revolutions is reached (rerun baseline test after every 2x ConOps revolutions).

TC4 – ConOps Testing: Incorporate a dust cup with a newly assembled actuator, perform ConOps testing with nominal load cases for each actuator, varying the temperature based on the rate as prescribed by thermal analysis (as hot as the chamber can allow). The testing would nominally follow this sequence:

1. Perform a functional run to compare to TC1
2. Run 32 dig and dump cycles, transitioning temperature at the expected mission rate. Starting temperature is the starting mission temperature for each actuator respectively.
3. Perform a functional run to compare to TC1.
4. Rerun steps 1 through 3.
5. Take out of chamber and disassemble to inspect seals.

III. Mobility Subsystem

The mobility subsystem (see Fig. 3) is responsible for moving IPEx along the lunar surface during operations and consists of wheels, wheel actuators, and supporting structure. During the 11-day reference technology demonstration mission, the mobility subsystem will transport IPEx at a nominal driving speed of 30 cm/s and a total distance of up to 70 km while traversing rock obstacles up to 7.5 cm in height and inclinations up to 15°. This driving rate is significantly higher than what has been accomplished by previous planetary rovers. Therefore, the design of the mobility subsystem is intentionally simple. The 4-wheel base uses a skid-steer approach that eliminates the need for steering actuators. There is no suspension system, and instead the wheels have a proportionally large diameter and width to allow for obstacle traversal. The following sections detail the design and testing of the mobility subsystem components.

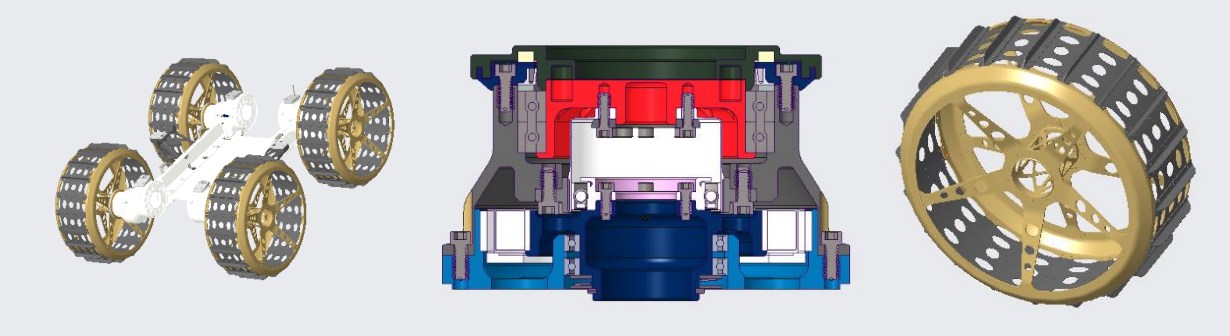

Fig. 3 Mobility subsystem components.

A. Wheel Actuator Design

Each of the four wheels are driven by custom actuators derived from the IPEx Generation 1 prototype (see Fig. 4). Keeping a simplistic approach was important during the design of the wheel actuators. The wheel actuator is made up of a brushless DC ThinGap LSI 75-12 motor with Honeywell SS511AT hall effect sensors, a Harmonic Drive CSF 14-80LW gearset, SKF 71809 angular contact back-to-back bearings on the output to react loads imparted into the actuator from the environment, EZO 6706 deep groove bearings for the motor rotor, and a Nomex dust seal.

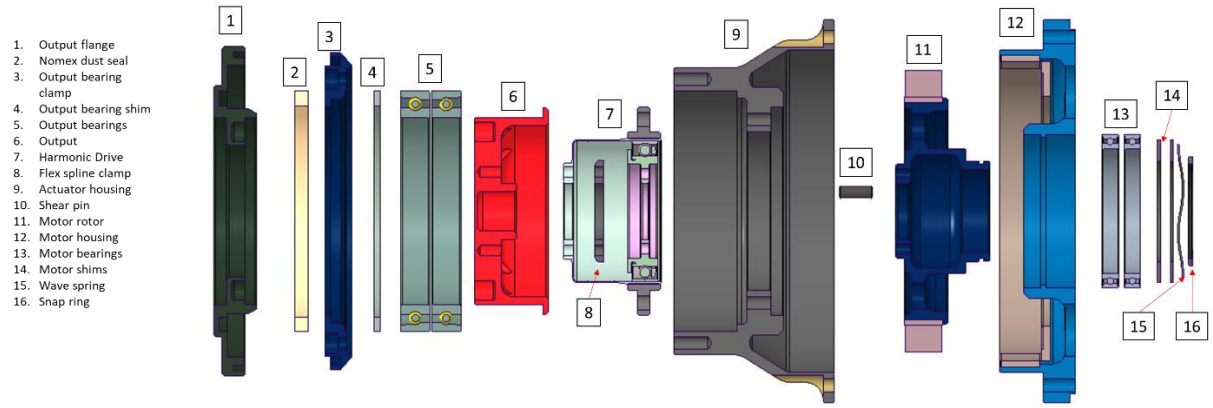

Fig. 4 Cross-section of wheel actuator.

Some of the load cases considered were driving over rocks with a height of 7.5 cm and below, driving at full speed with and without a regolith payload, and skid steer loads which included a rule of thumb that two actuators can provide enough torque to drive vertically up a wall. Listed below are the load cases used to size the actuator.

- **Case 1:** Robot hanging vertical on lander or rock face by only two wheels and holding position or actuating with full regolith payload. (Not probable case. but it is used as a rule of thumb when designing skid steer robots.)
- **Case 2:** Robot hanging vertical on lander or rock face by four wheels and holding position or actuating with full regolith payload.
- **Case 3a:** Driving unloaded on regolith in previously traversed terrain on two wheels. (Using RASSOR 2 data the team saw cases where only two wheel actuators were active.)
- **Case 3b:** Driving unloaded on regolith in previously traversed terrain on three wheels. (Using RASSOR 2 data the team saw cases where only three wheel actuators were active.)
- **Case 3c:** Driving/climbing over rocks at 1.32 cm height without regolith payload.
- **Case 4a:** Driving loaded on regolith in terrain on two wheels. (Using RASSOR 2 data the team saw cases where only two wheel actuators were active.)
- **Case 4b:** Driving loaded on regolith in terrain on three wheels. (Using RASSOR 2 data the team saw cases where only three wheel actuators were active.)
- **Case 4c:** Driving/climbing over rocks at 1.32 cm height loaded.
- **Case 5:** Driving while excavating.

- **Case 6:** Driving over a rock at 7.5 cm height loaded.

These load cases were used to select a gear ratio, type of gearbox and motor within the mass, volume, and power requirements. Table 3 below is a chart with each load case's torque, speed and duration of use according to the ConOps.

Table 3 Loads experienced by IPEx during ConOps.

Load Case	Gearbox load (N*m) 80:1 Gear Ratio	Motor load (N*m)	Motor speed (RPM)	~ConOps duration (hours)
Case 1	7.45	0.24	150	0.075
Case 2	3.77	0.148	150	0.075
Case 3a Case 3b Case 3c	0.528 0.346 1.435	0.065 0.063 0.093	1530 1530 1530	18 6 6.77
Case 4a Case 4b Case 4c	1.192 0.733 2.695	0.067 0.059 0.113	1530 1530 1530	18 6 6.77
Case 5	1.063	0.064	65	11.7
Case 6	5.581	0.198	1530	0.75

B. Wheel Actuator Testing

The TRL-5 wheel actuators were tested at KSC in the Swamp Works Space Environment Dynamometers (SEDs) [6] (see Fig. 5). These vacuum chambers use a ferrofluid rotary shaft to transfer a torsional load from a brake outside the chamber to the test article inside the chamber. A cryocooler is used to conductively remove heat from the test article.; Testing at a specific temperature is made possible using a closed-loop controller that utilizes heaters and temperature sensors. This setup allows the test article to be tested in vacuum, at the appropriate temperature, under a specific load, and with regolith simulant.

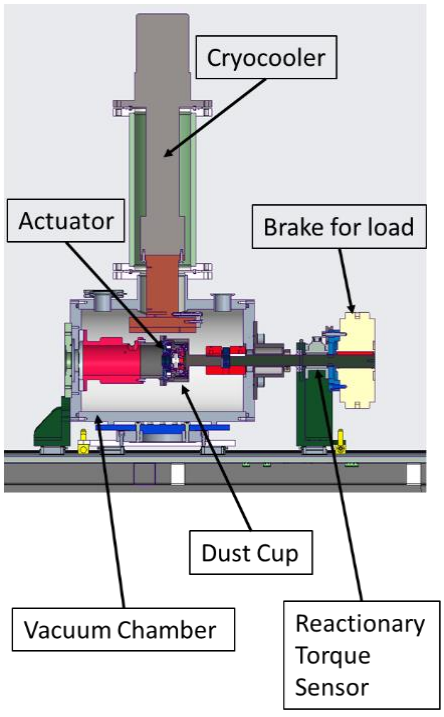

Fig. 5 Wheel actuator in space environment dynamometer.

A major goal of the testing was not only to demonstrate that the actuator can perform in the lunar environment but also to characterize the performance in all aspects of the environment. This will enable the team to use the telemetry data during the mission to better understand the loading condition on the Moon. By analyzing telemetry such as current draw on the actuator, battery voltage and current, temperature and speed, the team can use the data collected during testing to understand the loads applied to the actuator, predict lifetime expectations, and identify potential faults. This data will be used to inform future mission designs.

Extensive testing on the wheel actuator was performed. TC1 and TC2 tests swept through a range of torques, speeds, battery voltages, and actuator surface temperatures, while active current, temperature, and voltage were measured. Torque ranges imparted were from 0 N*m to 15 N*m at 3 N*m intervals. Input speed ranges were 10 RPM, 25 RPM, 50 RPM, and 100 RPM to 1700 RPM at 200 RPM intervals. TC2 reperformed the characterization but at -35 and 40 °C surface temperatures. It was found that varying the voltage at 47.6 V, 53.2 V and 58.8 V resulted in negligible effects of motor response.

The results of these tests were used to derive an equation that can predict the loads on the actuator based on voltage, speed, temperature, and active current (see Fig. 6). This equation and the results will feed back into the scaling and sizing analysis to validate the sizing and power estimates. Below is a graph of the wheel actuator characterization and the equation to predict loads during the mission.

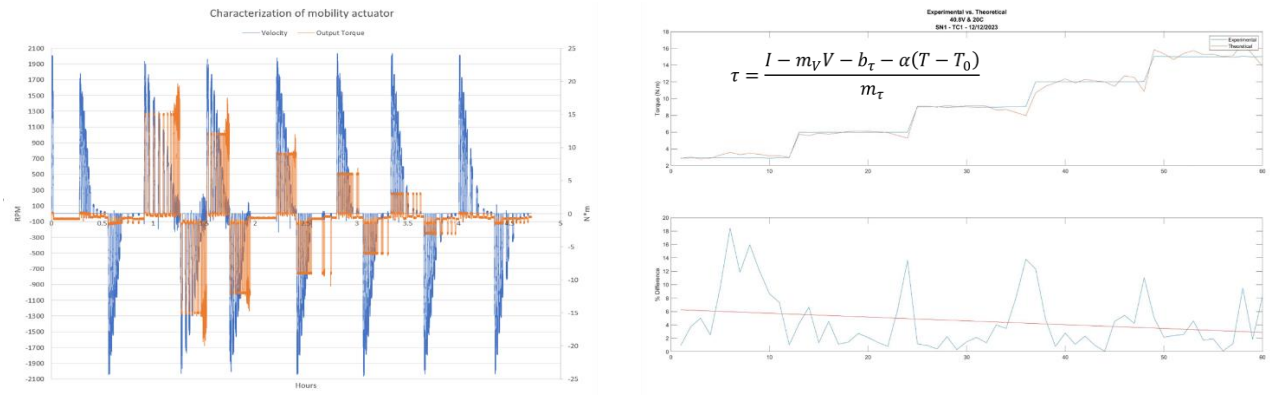

Fig. 6 Typical motor characterization data and curve fit equation.

TC3 - Accelerated life testing of the wheel actuator used a 3-sigma accelerated profile. The 3-sigma load was based upon the nominal max load during operation, which corresponds to driving over a 1.32 cm tall rock. This rock size is a mean rock size taken from a lunar rock distribution in the IPEx Environmental and Mission Operations Specification (EMOS). The goal of the accelerated life testing was to achieve a minimum 1x mission input revolutions, but ultimately continue to failure. The IPEx mission ConOps requires 5.7 million input revolutions.

Several issues occurred during the test, all of which were due to motor current limits reached. After investigating the cause of the fault, the team determined that the wave generator was moving axially into the flex cup, causing the springs on the motor rotors bearings to fail. In total, the wheel actuator did successfully operate for over 1x mission input revolutions (6,547,036 input revolutions) over multiple inspections and disassembly.

Due to the axial movement of the motor rotor and the failure of the motor rotor bearing, this test proves additional testing and design changes are required. Future work includes modifying the grease application on the harmonic drive to improve lubrication between the flex cup and the wave generator band.
Fig. 7 below shows the life of the test and power draw when failures began.

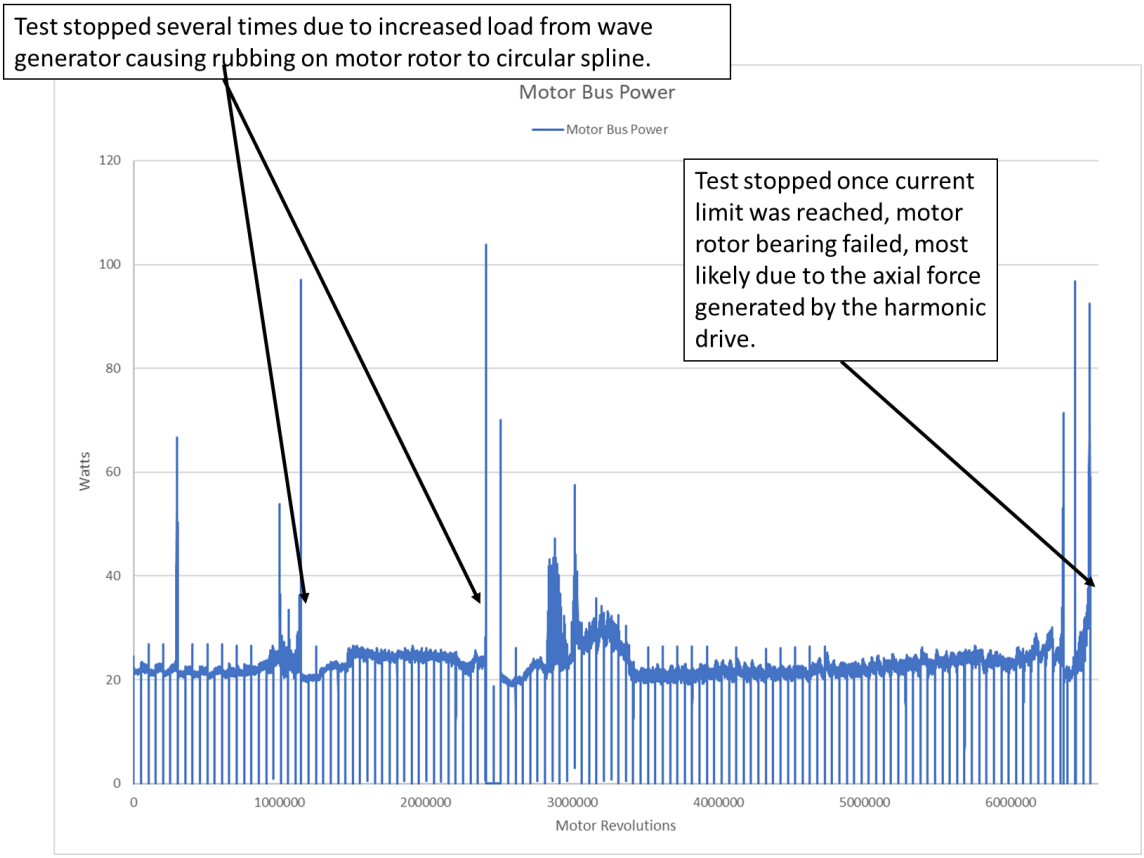

Fig. 7 TC3 accelerated life test of wheel actuator.

The TC4 tests were performed with a “test as you fly” approach recreating the thermal profile and regolith interaction the actuators will encounter during the lunar mission. This testing demonstrated that a single felt seal provided sufficient protection from the regolith dust in a worst-case scenario. Minimal dust was found beyond the felt seal, though a significant amount of dust penetrated the labyrinth portion of the seal (see Fig. 8). This occurred due to the way the dust was applied while the actuator was running. A dust cup was attached to the output of the actuator and constantly conveyed dust over the top of the interface of the rotating output and submerged the lower section of the actuator. It is thought that submerging the actuator caused the dust to migrate into the labyrinth.

Simulant: OPRH4W30, Highland Regolith Simulant with 30% Agglutinates

Dust Cup removal. Simulant deposition post testing.

Felt Seal after 5,880,000 inputs rev with simulant. (73,500 output revs)

Output bearings behind felt seal. Very little dust intrusion past felt seal.

Fig. 8 Wheel actuator regolith seal testing.

Although dust entered that part of the actuator, it still successfully performed the entire ConOps. Below is a chart of the TC4 test profile in Table 4 and a graph of the results, in Fig. 9. The red boxes and line are identical portions of the test. There is a slight increase in power draw from the beginning to the end, but it is negligible.

Table 4 TC4 mobility ConOps profile.

Step	Load (Nm)	Speed (rpm)	Ramp (rpm/s)	Duration (motor revs)	Duration (output revs)	Cases	Notes
Perform No Load at Ambient Temperature (Pre-test)							
0	0	+1000	100	+1000	+6.66	Pre-Test No Load	Check out at beginning.
Test starts at -35C (Initial temperature set point +/- 5C, free error margin for other temperatures) 40.8 volts							
1	1.5	+1530	100	+8500	+106.25	Torque to drive to excavation site	Torque predicted while driving over rocks unloaded.
2	1.1	+64	100	+135	+1.6875	Torque to drive while excavating	Torque predicted while excavating.
3	2.7	-1530	100	-8500	-106.25	Torque to drive to dump site after excavation	Torque predicted while driving over rocks loaded.
4	Repeat steps 1 through 3 (10.82 min per cycle) 7 times						
5	Increase temperature by 5C						
6	Go back to Step 4 (until 45C is reached and move to step 7)						
7	Set 45C and repeat steps 1 through 3 (10.82 min per cycle) 112 times						
8	Decrease temperature by 5C						
9	Repeat steps 1 through 3 (10.82 min per cycle) 9 times						
10	Decrease temperature by 5C						
11	Go back to step 9 (until -15C is reached)						
12	0	+1000	100	+1000	+6.66	Intermediate Temperature No Load	Runs for 15 min
Exit criteria: Test completes							

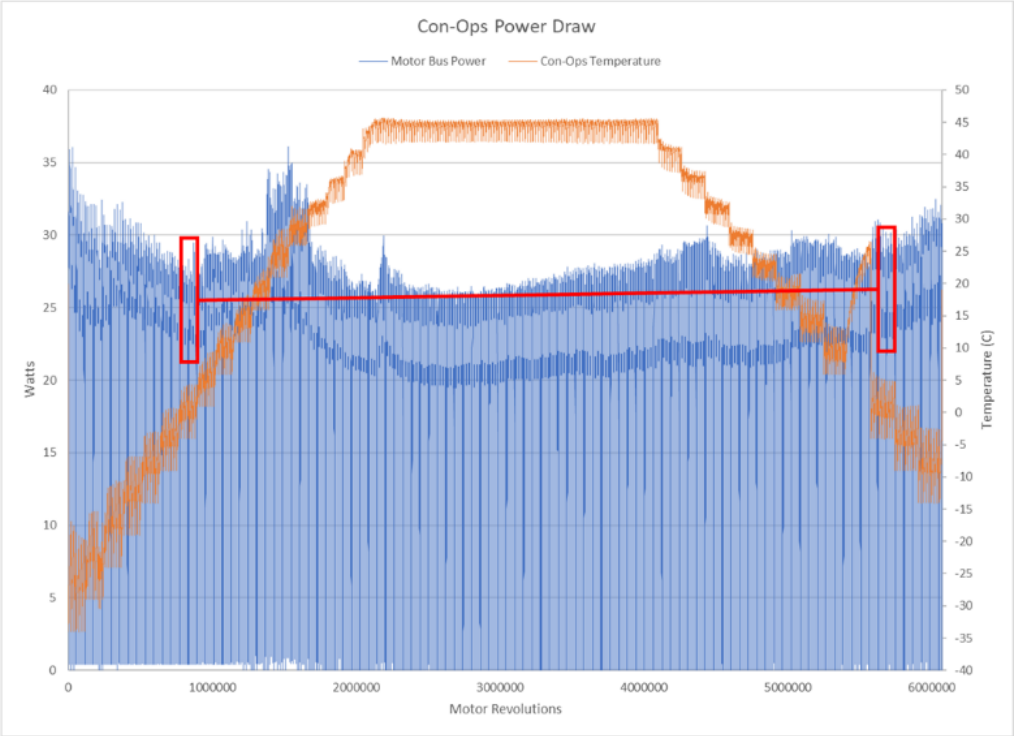

Fig. 9 TC4 mobility ConOps Results.

C. Wheel Design

The wheel design began as a modified version of the wheels being used on the Volatiles Investigating Polar Exploration Rover (VIPER) [7], with unique features for IPEx's skid-steer driving approach. IPEx's wheels needed to be very robust due to the nature of the mission and the 70 km distance IPEx is expected to cover during the 11 days on the lunar surface. Although a trade study was conducted as mentioned below, the wheels needed to be modular so that components could be replaced as testing on the full scale IPEx progressed. The grousers, cleat surfaces and spokes were designed to be removable and changed. The side rings were designed with a large, chamfered edge to act as a "ski" during skid steer turning. This feature prevents the wheel's edge from digging into the regolith while turning, which would otherwise increase lateral and torsional forces. A hard coat anodize was used on the grousers and cleat surfaces to combat the abrasiveness of the lunar regolith, while the side rings, spokes, and hubs received a chemical conversion coating to prevent corrosion and allow for electrical grounding (see Fig. 10).

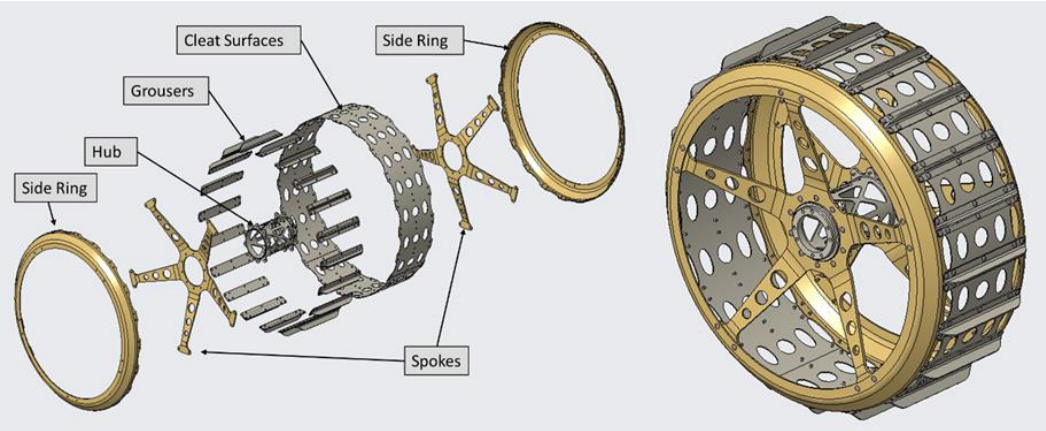

Fig. 10 IPEx wheel design.

The wheel dynamic load cases (driving load case for wheel reliability) assume 30 cm/s and traveling over rocks 7.5 cm tall or shorter without slowing down. The cases are as follows:

Dynamic Load Case 1:
IPEx supported on two wheels (left front and right rear)
Step 1: 1g (earth) static load applied. Allows all components to be in proper deformed state prior to impact.
Step 2: Left front wheel displaced up 75 mm in 0.437 seconds.
- Calculated travel time assuming IPEx does not slow down as the wheel hits a vertical rock 75 mm tall.

Step 3: Left front wheel held at 75 mm high for 0.163 seconds to let impact distribute through the vehicle.

Dynamic Load Case 2:
IPEx supported on two wheels (left front and right rear)
Step 1: 1g (earth) static load applied. Allows all components to be in proper deformed state prior to impact.
Step 2: Left front wheel displaced up 75 mm in 0.437 seconds.
- Calculated travel time assuming IPEx does not slow down as the wheel hits a vertical rock 75 mm tall.

Step 3: robot falls off rock with 1g (earth) applied. The left front wheel in free-fall until impact with rigid ground approximately 0.113 seconds later.
- 7.5 cm fall on earth equivalent to 45.0 cm fall on lunar surface. While conservative, this event will be observed during earth testing, and a similar fall may be observed during deployment of IPEx.

Step 4: loads allowed to distribute throughout vehicle for 0.2 seconds.

D. Wheel Testing

To select a wheel design for the TRL-5 IPEx, a short trade study was conducted by testing various wheel geometries while driving the RASSOR 2 system in BP-1 lunar regolith simulant. The methodology and results from this trade study are described in this section, with more details available in [8]. The study compared the behavior of different grousers (traction-enhancing protrusions) and cleat (tread pattern) wheel designs. Ten wheel geometries were tested in four distinct scenarios: 1) driving in a circle with increasing diameter, 2) driving in a straight line with increasing velocity, 3) slope driving up a 20° incline, and 4) drawbar pull. The RASSOR 2 platform measured wheel encoder readings, robot pose via the Opti Track motion capture system, and bus power. Fig. 11 depicts RASSOR 2 excavator installed with a prototype wheel concept.

Fig. 11 RASSOR 2 excavator with IPEx concept test wheels.

Ten different wheel configurations were tested during this campaign. Below is a visual summary highlighting the differences for each wheel. Note that while eight designs are shown below, the tapered cleat/holes + tapered 6.5 and

12.9 mm grouser wheel configurations were each repeated with every other cleat removed, resulting in ten discrete configurations tested (see Fig. 12).

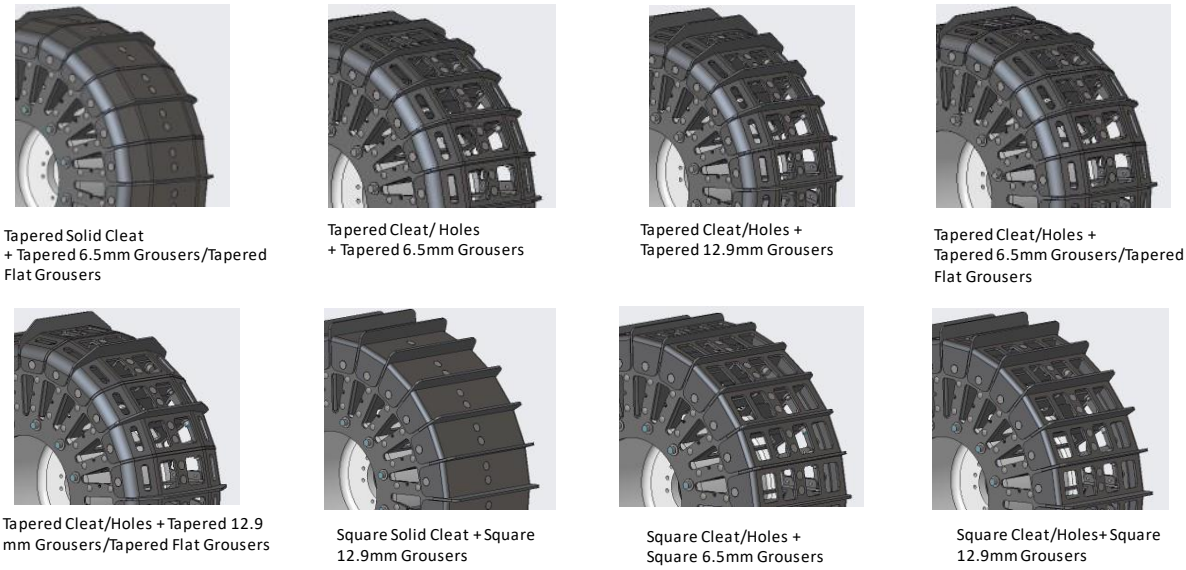

Fig. 12 Different configurations of each wheel tested.

The data collected during testing was used to evaluate the slip rate and power usage for each wheel design as metrics of overall performance. Wheel slip was defined by subtracting the "ideal" travel distance (from the wheel encoders) from the "actual" travel distance (from the motion capture system). Fig. 13 below shows an example graph of wheel slip over time. Slip rate was defined by calculating the slope of this relationship using linear regression.

After analyzing the data, several key findings were identified which aided in the design and selection of the IPEx wheels. First, a tradeoff was evident between slip rate and power usage. Short, tapered grousers had higher slip rates than long square grousers but consumed less power while driving. Next, the grouser design affected the wheel performance differently based on the test scenario. Short grousers had lower slip rates than long grousers in straight line driving tests, but their performance worsened for the circle driving tests as the turn radius decreased. Tapered grousers showed a similar trend in comparison to square grousers but generally performed slightly better across all tests. Finally, the cleat design did not significantly impact wheel performance. The removal of alternating cleats resulted in higher slip rates and power consumption, while solid cleats and cleats with holes performed similarly in all tests. Fig. 14 shows the overall performance results, including actual velocity (which is negatively related to slip rate) and power consumption for each wheel design.

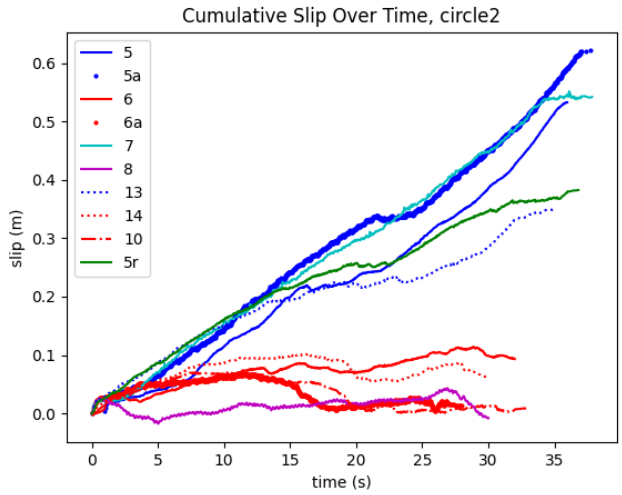

Fig. 13 Example graph of wheel slip over time for a circle driving test.

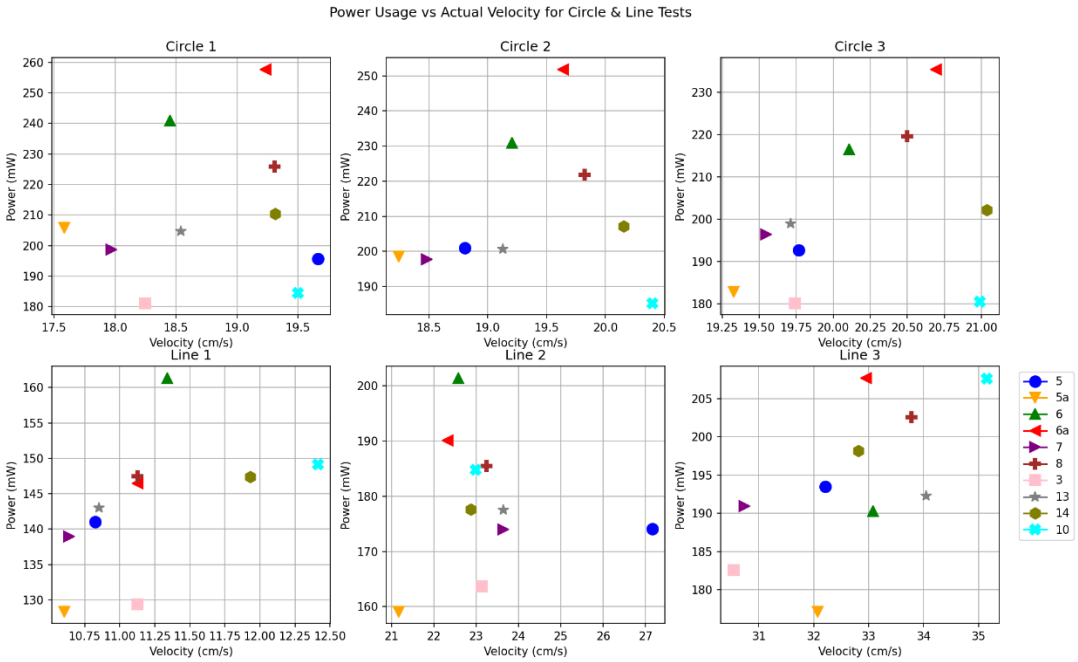

Fig. 14 Overall performance graph for circle and line driving tests.

Given that the dynamic load case was producing shock values above expected levels for an 11-day mission, a test was conducted on the prototype aluminum wheels using RASSOR 2. The test consisted of driving over basalt rock measuring between 7 and 10 cm high (height variable across the top of rock) with accelerometers placed on the actuator housing of the impacting wheel, electronics bay, and shoulder joint near the interface of the bucket drum arm . The purpose was to validate the shock data observed in the finite element analysis (FEA) dynamic load case (see Fig. 15).

Results indicated a significant discrepancy between the FEA results and the actual results, with two caveats. The testing represented a single use case among many possible scenarios, and it was not conducted at temperature and with the selected wheel design. However, this load case assumes Earth gravity, while lunar gravity shows less impact loading.

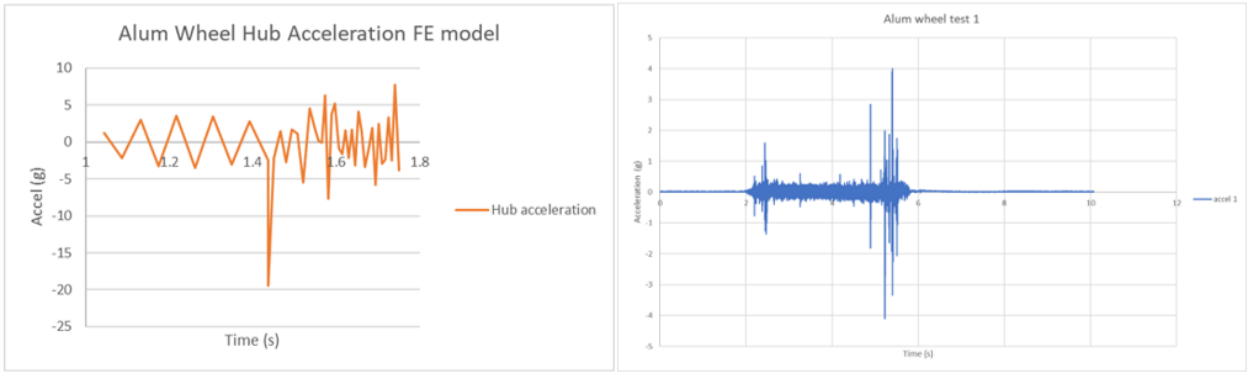

Fig. 15 Wheel dynamic load case analysis vs test.

Given these results, the team decided to proceed forward with the rigid aluminum wheel as described, while keeping an alternative design ready in case future testing alters the risk posture of using the rigid aluminum wheel.

IV. Regolith Delivery Subsystem

The regolith delivery subsystem (see Fig. 16) is responsible for collecting, holding, and depositing regolith during operations. It includes the bucket drums, bucket drum actuators, arms, and arm actuators. During the 11-day reference technology demonstration mission, the subsystem will collect, store, and deposit up to 30 kg of regolith per excavation cycle throughout the mission, with a minimum success threshold of 15 kg. It will also support mass measurements via the motor currents produced by the arm actuator to verify regolith collection rates. Over the mission's duration, this will amount to moving a total of 5,000 to 10,000 kg of regolith moved.

The end-effectors of the regolith delivery subsystem are a pair of bucket drums that rotate to excavate the surface regolith and contain it via an internal baffle system until deposition. Both bucket drums are controlled by a single bucket drum actuator that is fixed to an arm, which is also controlled by a single arm actuator. The arm and arm actuator allow IPEx to control the dig depth of the bucket drums, which ensures proper force balancing between the front and rear bucket drum pairs. This is achieved using an autonomous excavation routine known as 'auto-dig' [9]. The forces required to actuate the bucket drums and the arm for excavation purposes exceed the forces needed to lift the rest of the IPEx system. Consequently, the regolith delivery system can enable extreme mobility modes where IPEx uses the bucket drums as a second set of wheels, lifts the chassis off the ground (to support activities like recharging and deployment), climb obstacles significantly taller than the wheels, and others.

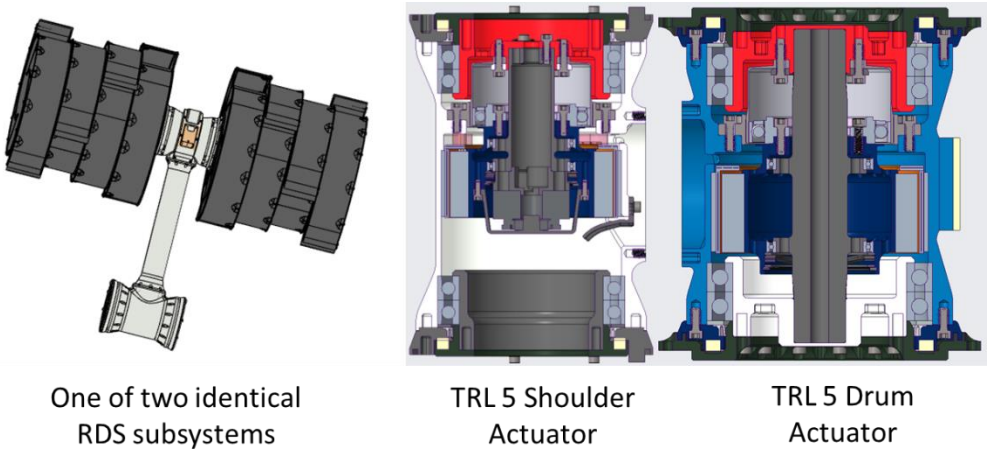

Fig. 16 Regolith Delivery Subsystem components.

A. Arm and Bucket Drum Actuator Designs

Two bucket drums are controlled by a single actuator that includes a Harmonic Drive CSF 20-160LW gear set, a ThinGap LSI 75-30 brushless DC motor with Hall effect sensors, deep groove ball bearings on the motor rotor, and

SKF 71812 angular contact bearings on the output. The bucket drum actuators have an internal shaft that transmits the torque from the output of the harmonic gear set to the opposite side of the actuator to facilitate rotating two bucket drums. The bucket drum actuator is mounted to a simple aluminum arm structure controlled by an arm actuator.

The arm actuator was designed to be nearly identical to the bucket drum actuator to reduce unique components and qualification times. The primary differences are that the arm actuator includes a power-off brake and lacks the internal torque-transmitting shaft. The brake keeps the arm from back-driving when power is not applied and will save energy while driving between dig and deposit operations. The ThinGap motor is the same diameter as the wheel actuator's motor allowing synergistic designs throughout. Fig. 17 shows a cross-section identifying the major components of the arm and excavation actuators.

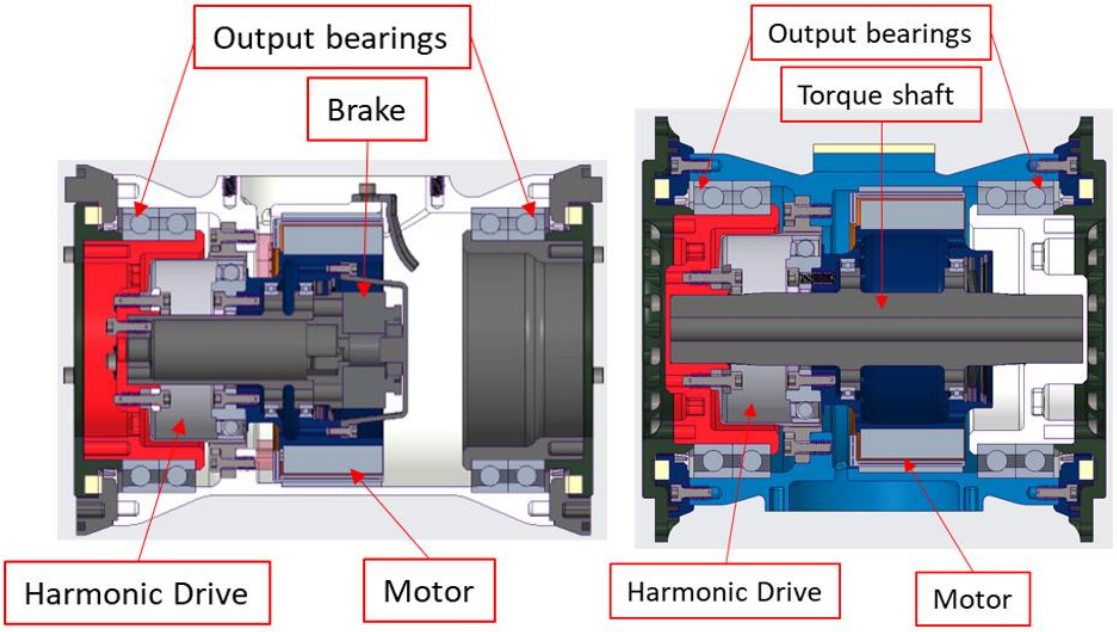

Fig. 17 Regolith Delivery Subsystem actuator cross-sections.

Loads imparted on the actuator were derived from the RASSOR 2 prototype just as the wheel actuator loads described above. Sizing of the motor and gear boxes resulted from the below load cases shown in Table 5 and Table 6 that were derived from the ConOps.

Arm actuator torsional load cases and resultant motor loads, speeds, and durations:

Case 1: Actuating the arm while digging with auto-dig routine.

Case 2: Hanging from the lander with only one drum attached to the lander.

Case 3: Fully loaded bucket drum moving to driving position.

Case 4: Empty bucket drum moving to digging position.

Case 5: "Iron cross" maneuver when arms are parallel to the ground. Assuming drums are locked in place. Typical operations include the drum rotating to match the arm speed. (This will be used when docking with the wireless charger.)

Table 5 Arm actuator load cases.

Load Case	Gearbox load (N*m) 160:1 Gear Ratio	Motor load (N*m)	Motor speed (RPM)	~Con-Ops duration (hours)
Case 1	18.58	0.26	460	11.73
Case 2	25	0.32	200	0.003
Case 3	13	0.23	260	0.43
Case 4	3.8	0.166	260	0.43
Case 5	24.7	.252	200	.2

Bucket Drum Actuator torsional load cases and resultant motor loads, speeds, and durations:
Case 1: Horizontal digging load during excavation.
Case 2: Hitting rocks while excavating.
Case 3: Peak load at end of excavation cycle (digging loads and tumbling regolith in drums).
Case 4: Dumping regolith.
Case 5: Offloading from lander (pull-up with the drum with dry mass).
Case 6: Driving on drums.

Table 6 Bucket drum actuator load cases.

Load Case	Gearbox load (N*m) 160:1 Gear Ratio	Motor load (N*m)	Motor speed (RPM)	~Con-Ops duration (hours)
Case 1	8.2	0.16	1066	11.7
Case 2	60.75	0.54	1066	2.6
Case 3	16.38	0.22	1066	0.18
Case 4	0.9	0.083	500	4.14
Case 5	7.5	0.155	500	0.003
Case 6	1.28	0.175	500	0

Based on these load cases and to maintain simplicity, the same motor, gear set, and bearings were selected. This reduced the part count in the design and allowed for a simplistic approach to manufacturing and testing.

B. Arm and Bucket Drum Actuator Testing

Both actuators have been fabricated and assembled and are undergoing TRL-5 testing in the SED chamber to characterize their lifetime and performance. The test setup, as shown in Fig. 18 and Fig. 19, involves adding heaters to the actuator's outer surface and wrapping the housing with copper straps to conductively cool the actuator when attached to the cryocooler. The combination of heaters and the cryocooler allows for precise temperature control during tests. A regolith conveying output shaft is used to pick up and deposit regolith dust from a dust cup fixed to the housing. This enables continuous dust deposition over the top of the actuator during TC4 ConOps tests. This testing also produced a dataset used to create a model of the actuators across various speeds, torques, temperatures, currents, and voltages. This model is in-turn used to predict the actuator's torque to estimate the amount of regolith inside the bucket drums and the force of excavation while digging.

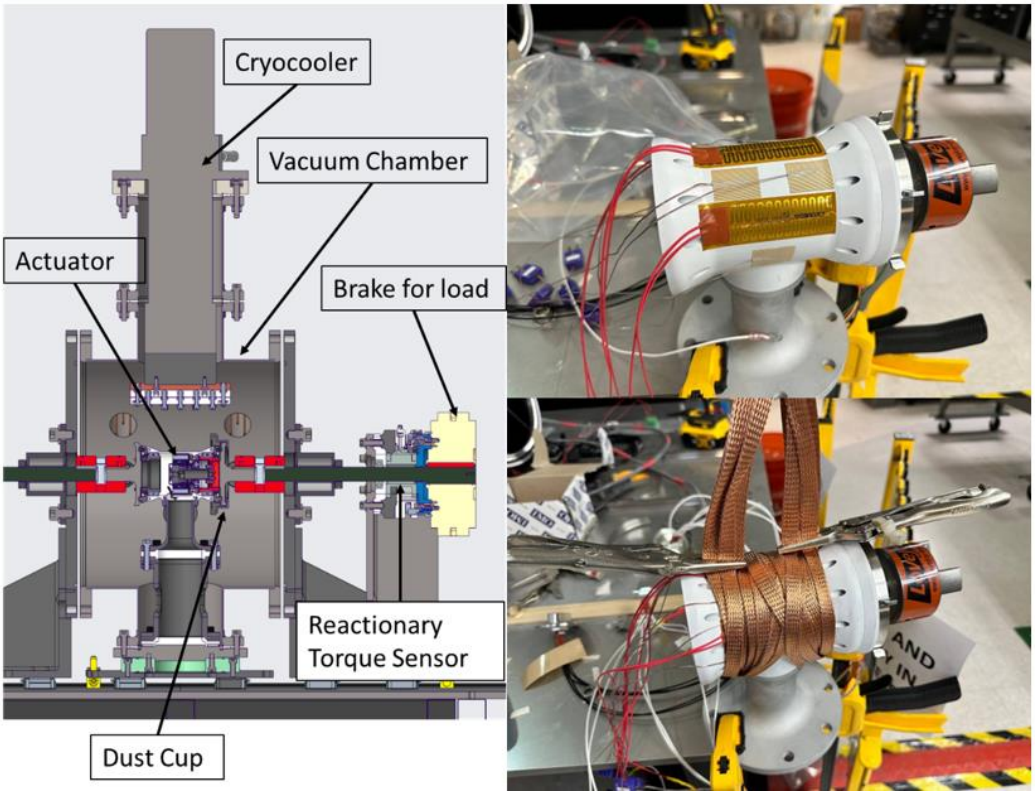

Fig. 18 Arm actuator test setup CAD (left) and actual heater and thermal strapping (right).

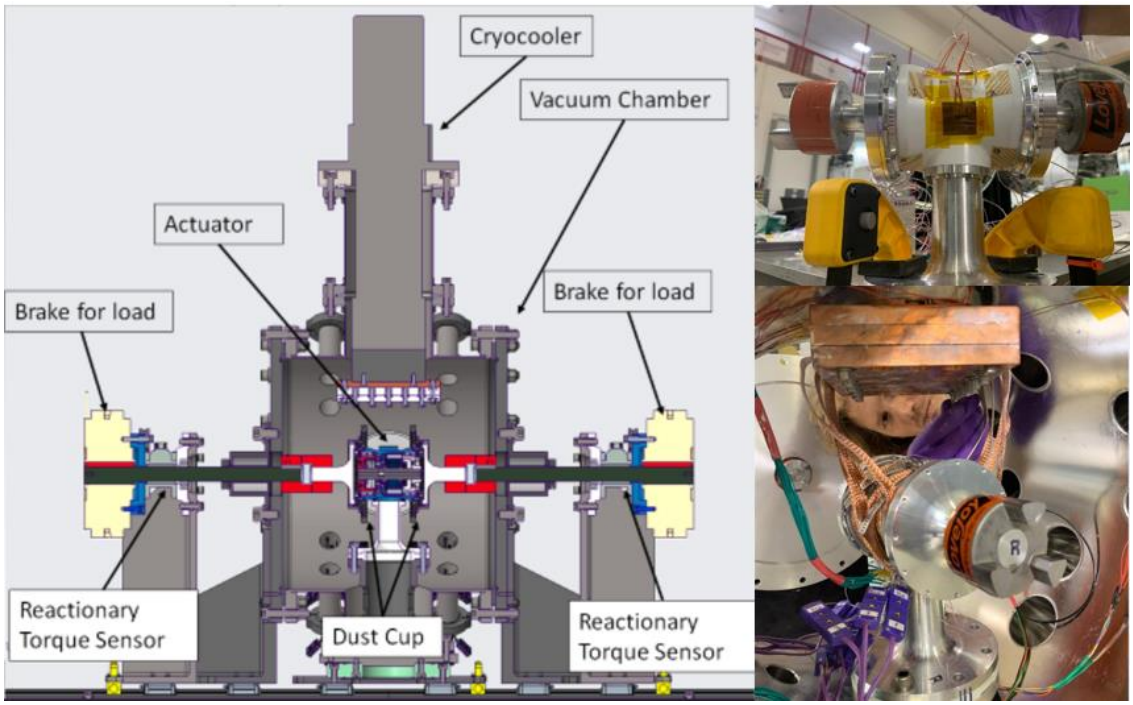

Fig. 19 Bucket drum actuator test setup CAD (left) and actual heater and thermal strapping (right).

The arm and bucket drum actuator test campaigns were performed in the same manner as the wheel actuator. TC1 and TC2 tests involved actuator performance characterization tests with thermal cycling to derive an equation for current related to torque draw at specific mission parameters. These tests covered a range of torques and speeds while recording active current, temperature, and voltage. Torque input to the actuator ranged from 0 to 50 N*m in 5 N*m intervals, and speed ranged from 200 to 2000 RPM in 200 RPM intervals. Fig. 20 shows an example graph of the bucket drum actuator's response during these tests.

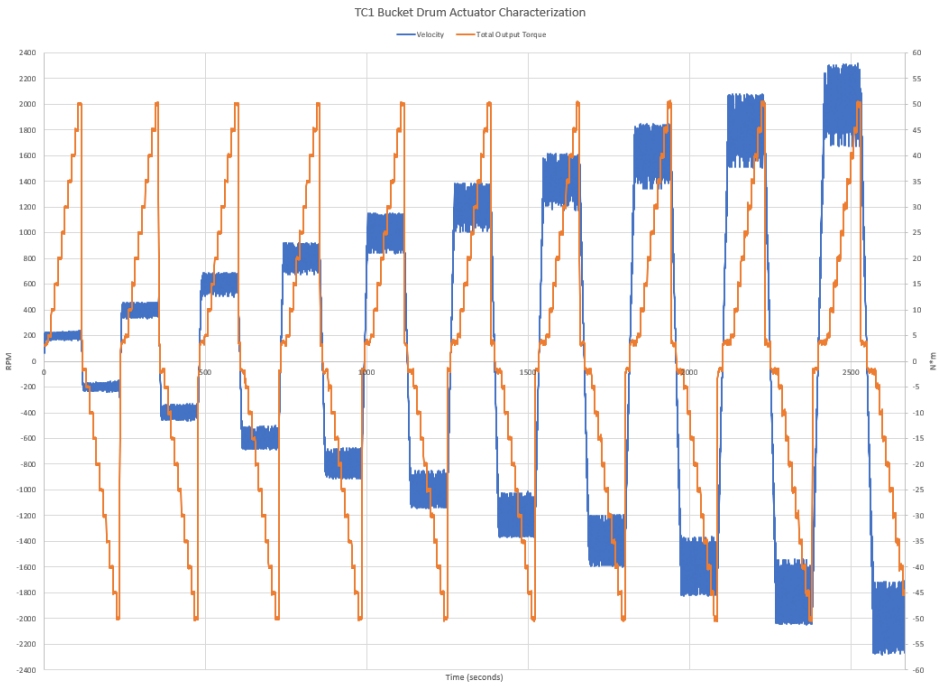

Fig. 20 Bucket drum actuator velocity and torque during TC1 testing.

The TC3 accelerated life test used a 2-sigma accelerated profile. The arm actuator's 2-sigma load was based on the nominal max loading during operation, which corresponds to digging while actuating the arm. The goal of the accelerated life test was to achieve a minimum 1x mission input revolutions, though ultimately continuing until failure. The IPEx mission ConOps requires approximately 337,000 input revolutions in a cyclic manner, rotating from 0 to 90° with the parameters described in Table 7.

Table 7 Arm actuator TC3 profile.

Step	Load (Nm)	Speed (rpm)	Ramp (rpm/s)	Duration (motor revs)	Notes
0 load represents the minimum load of the test stand. Temperature: Ambient (25C +-10C) Ramp load 5 N*m per second Minimum voltage: 40.8 Volts 675,535 motor revolutions = 2x life					
0	0	500	100	10 sec	
1	18.5	+500	100	100,000 motor revolutions	18.5 Nm is predicted excavation load on the moon
2	18.5	-500	100	100,000 motor revolutions	
3	Continue Steps 1 and 2 until failure or 2,000,000 motor revolutions are reached				
4	If 2,000,000 motor revolutions are reached run Step 0				

In total, the arm actuator successfully operated for over 4x mission input revolutions (1,402,223 input revolutions) without any issues. The graph in Fig. 21 shows an increase in power towards the end of the test but the first 3x ConOps cycles meet the requirements of the test. The test was stopped at this point to move on to the TC4 testing.

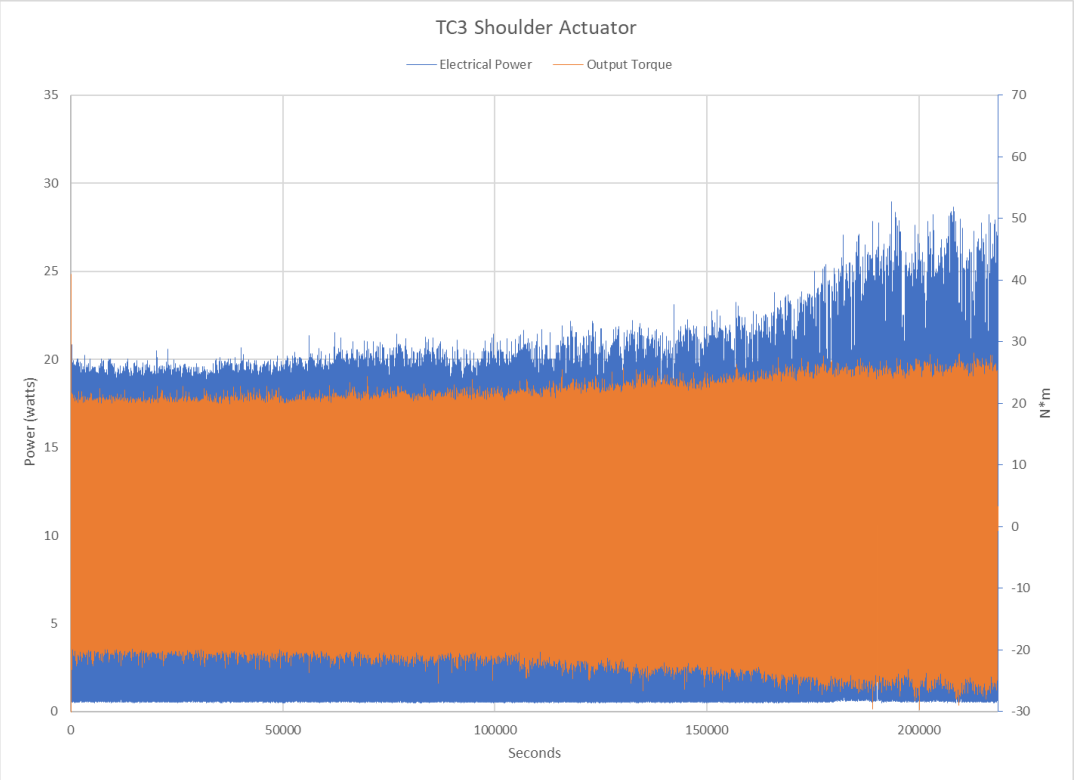

Fig. 21 TC3 arm actuator accelerated life test

The TC4 ConOps testing incorporated a dust cup with the previous actuator used for TC1, TC2, and TC3. Keeping the same actuator build for ConOps testing was not ideal but was decided upon due to time constraints. The temperature varied based on the rate prescribed by a transient thermal analysis, ranging from -35 to 40 °C. The testing would nominally go as follows:

1. Perform a functional run to compare to TC1.
2. Run 32 dig and dump cycles (analogous to the required number of cycles), transitioning temperature at the expected mission rate per thermal modeling. Starting temperature is the starting mission temperature for each actuator respectively.
3. Perform a functional run to compare to TC1.
4. Rerun steps 1 through 3.
5. Take out of chamber and disassemble to inspect.

The test parameters shown in Table 8 were devised to mimic the expected movements during the mission. This included a portion of the test that replicates the auto-dig routine, which raises and lowers the arm with the arm actuator while an algorithm maintains constant force on each side of the excavator. To mimic this movement, a cyclic 4.5 input revolution was used to switch directions.

Table 8 TC4 test parameters for arm actuator.

Step	Load (Nm)	Speed (rpm)	Ramp (rpm/s)	Duration (motor revs)	Duration (output revs)	Cases	Notes
Test starts at -10C (Initial temperature set point +/- 5C, free error margin for other temperatures) 40.8 volts							
0	0	+500	100	+500	+3.125	Check out at beginning.	
1	25	+200	100	+40	+0.25	Offloading from Lander	0 to 90 degrees (40 input revs)
2	3.8	-260	100	-20	-0.125	Unloaded 45deg to 0 deg	
3	18.5	+500	100	+4.5	+0.028	Excavating	
4	18.5	-500	100	-4.5	-0.028	Excavating	
Repeat Steps 3 through 4 112 times							
5	13	+260	100	+20	+0.125	Loaded 0 deg to 45 deg	
6	**Repeat steps 2 through 5 18 times**						
7	**Increase temperature by 5C**						
8	**Go back to Step 6(until 20C is reached)**						
9	**Hold 20C and repeat steps 2 through 5 115 times**						
10	**Decrease temperature by 5C**						
11	**Repeat steps 2 through 5 22 times**						
12	**Go back to step 10 (until -5C is reached)**						
13	0	+500	100	+500	+3.125		
Exit criteria: 1x ConOps complete							

Preliminary results from the TC4 test are shown in Fig. 22. The graph illustrates the cyclic movement of the actuator during the test. Each of the cycles switch directions 224 times per cycle.

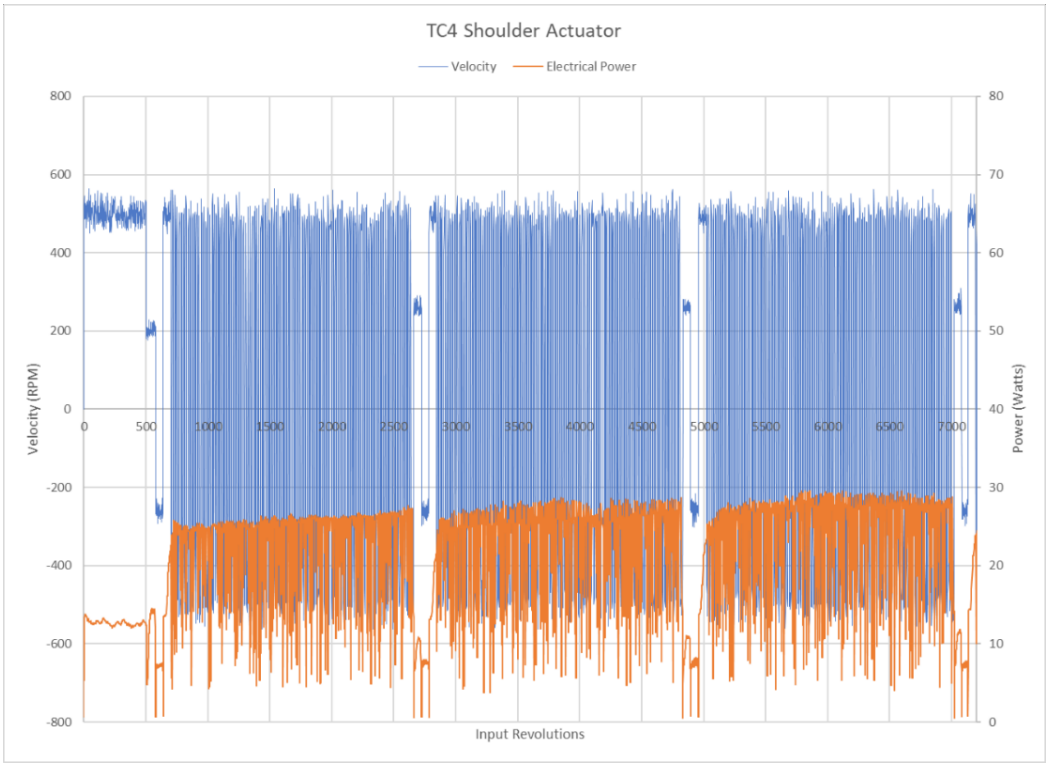

Fig. 22 TC4 arm actuator test showing 3 of 93,296 cycles.

C. Bucket Drum Design

The bucket drum design is a modification of the RASSOR 2 design and features a billet aluminum construction [10]. The bucket drums (see Fig. 23) are divided into four sections, with each section fabricated as a separate part and then fastened together with bolts. The shape of the bucket drums follows an expanding spiral, like that of RASSOR 2. However, an experiment to evaluate various geometries under simulated lunar gravity and vacuum is expected to fly in 2024 (see Fig. 25 and Fig. 26), and future iterations of the bucket drums will incorporate the optimized geometry. The goals of the drums are to efficiently collect regolith, contain the collected regolith while IPEx drives over lunar terrain, and dump the regolith. The drums should be optimized to minimize power consumption during digging and dumping and to reduce complexity, cost, and manufacturing difficulty.

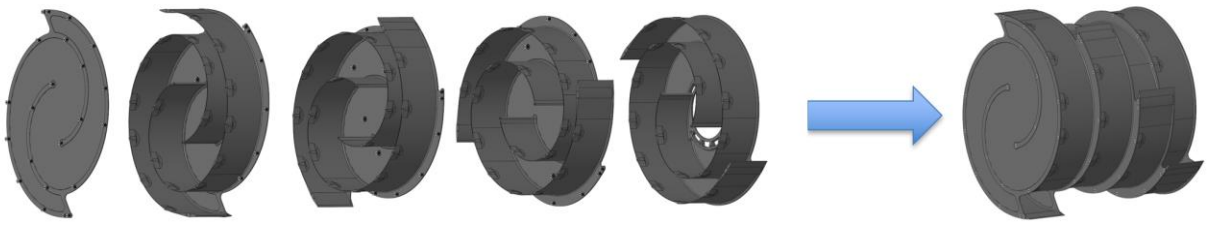

Fig. 23 IPEx TRL-5 bucket drum assembly CAD.

D. Bucket Drum Testing

Past bucket drum experiments included scaling down the RASSOR 2 bucket drum design to both minimal and maximal IPEx-sized bucket drums to observe how their size affected digging and collection performance. This helped determine how scaling a bucket drum impacts torque loads experienced by the actuators, so that they can be sized accordingly [10].

To understand regolith flow through different bucket drum spiral geometries, a Discrete Element Modeling (DEM) study was conducted. This study focused on spiral geometry and measured the total regolith mass collected as the primary performance indicator. From these simulations, the straight spiral and diverging spiral geometries (Fig. 24) were selected for further testing in an upcoming flight experiment.

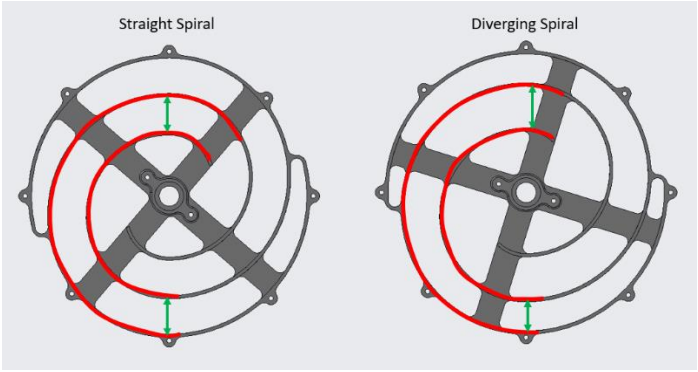

Fig. 24 Bucket drum straight spiral & diverging spiral geometries.

The experiment will fly on a Blue Origin New Shepard suborbital velocity flight in late 2024. Once in microgravity, the payload will be subjected to a centrifugal force from the capsule's rotational velocity to simulate lunar gravity for two minutes. The experiment will consist of six bucket drum slices inside a vacuum chamber, each containing either regolith simulants of varying particle size distributions (coarse, mid, or fine particles) or glass beads. The purpose of the experiment is to ensure that regolith flows as expected in a lunar gravity and vacuum environment and to identify potential issues with regolith jamming inside the bucket drums. After the experimental data is collected, a DEM study will be conducted using the same experimental parameters to validate the model for future use.

The assembly consists of a custom vacuum chamber that can hold three bucket drums each. There will be two lockers on the suborbital flight, accommodating a total of six bucket drum experiments. Each bucket drum is enclosed with regolith or beads as outlined in Table 9. Motors inside of the vacuum chamber will independently rotate each

bucket drum, causing the regolith to flow. Data will be captured via cameras positioned over the bucket drums for processing post-flight. The data collected from this experiment will be included in a future publication.

Table 9 IPEx bucket drum experimental payload test matrix.

Drum Number	Spiral Geometry	Simulant Type
Drum 1	Straight	Mid
Drum 2	Diverging	Mid
Drum 3	Straight	Coarse
Drum 4	Straight	Beads
Drum 5	Straight	Fine
Drum 6	Diverging	Coarse

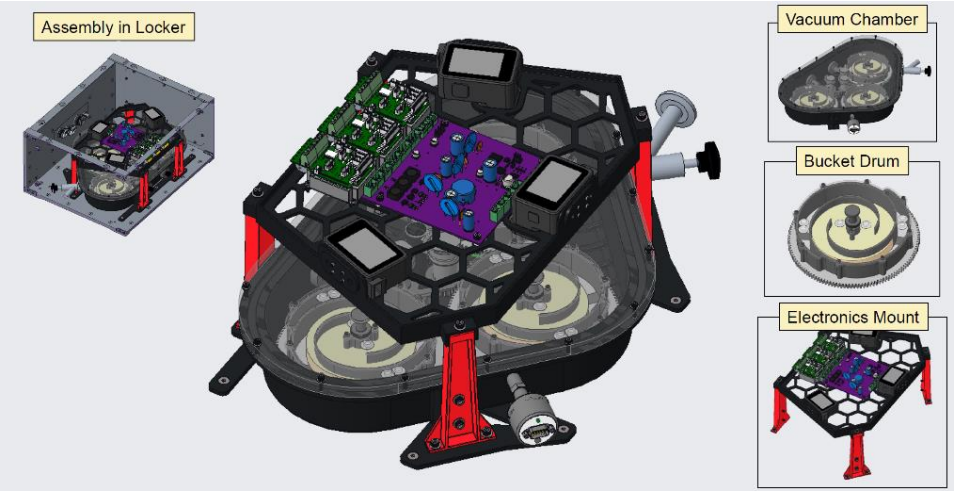

Fig. 25 IPEx bucket drum experimental payload overview.

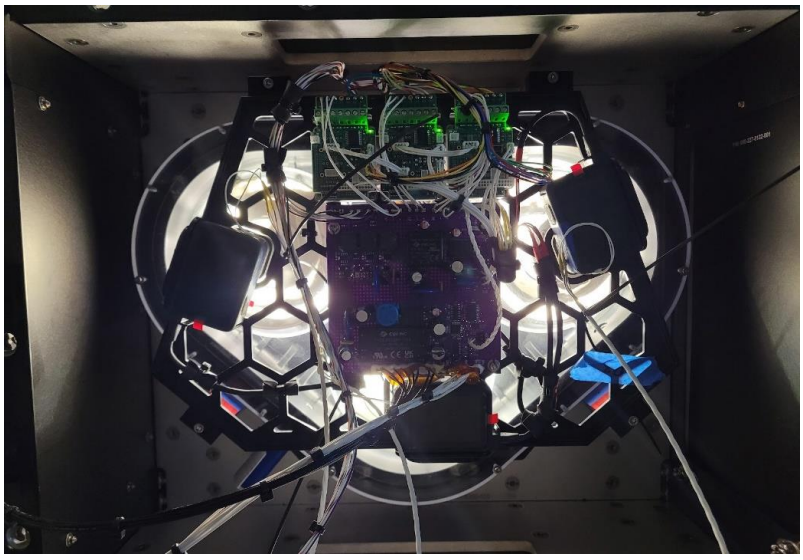

Fig. 26 IPEx bucket drum experimental payload final assembly.

V. Camera and Dust Mitigation Subsystem

The camera and dust mitigation subsystem is responsible for providing the imagery needed for navigation and operations and includes the camera sensors, lenses, illumination, and dust mitigating lens covers.

IPEx uses cameras for localization and situational awareness. The minimum number of cameras IPEx needs to operate are four and include one stereo pair, one side-facing, and one between a set of bucket drums. The stereo pair enables visual odometry and hazard identification, the side-facing camera primarily tracks the location of the lander, and the camera between the bucket drums provides views of the terrain and excavator itself (Fig. 27). The following sections detail the selection, design, and testing of the camera and dust mitigation subsystem components.

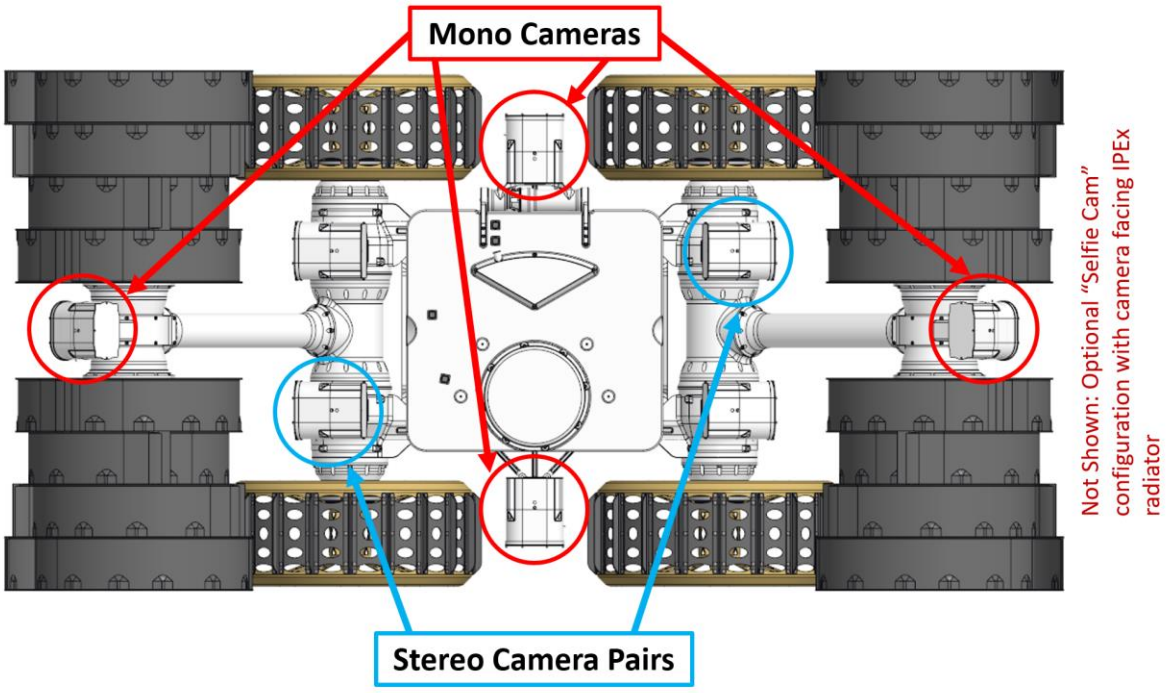

Fig. 27 IPEx camera types and locations.

A. Camera Sensor, Lens, and Lighting Selection

When designing a stereo camera system for robotic navigation, several factors need consideration. IPEx uses a navigation and localization strategy that relies on stereo imaging for depth estimation. In the absence of a global positioning system (GPS), the cameras are also utilized to recognize landmarks, such as the lander, to estimate the robot's pose. When choosing parameters for the camera system to best suit the various vision subsystems, optimizations must be balanced to ensure the performance of the vision strategies, which may have conflicting needs. For example, while a wider field-of-view (FOV) benefits near sighted hazard detection and visual odometry, a narrower FOV improves pose estimation when observing a distant lander. The key specifications to determine are:

- Quantity of monocular and stereo cameras
- The camera's position relative to the robot
- Sensor resolution and pixel size
- Lens focal length
- Lens aperture
- Stereo baseline and angle
- Monochromatic/color

Adjustments to each of these parameters has an impact on many different aspects of the resultant camera system's capabilities, most notably they affect:

- The hyperfocal distance and depth of field

- The camera FOV
- The depth estimation accuracy at various distances
- The "near sightedness" of the system, i.e. how close to the camera depth estimation

1. Sensor & Lens Class Selection

A 5-megapixel (MP) camera sensor was chosen to balance visual fidelity and performance of the computer vision software. This resolution ensures sufficient pixel accuracy for pose estimation at range within the constraints of on-board compute resources. For computationally demanding operations, images are downscaled to improve performance. Initial testing used a Sony IMX264 sensor with a pixel size of 3.45 µm with a commercial-off-the-shelf (COTS) C-mount lens. Various lenses and focal lengths were evaluated to understand their impact on robotic localization and FOV. However, COTS C-mount lenses posed challenges, including venting in vacuum, outgassing from adjustment mechanism grease, and increased complexity due to variable aperture and focusing mechanisms. To address these limitations, a simpler design with an S-mount lens was chosen. S-mount lenses typically feature a fixed aperture and simple mechanical design, with no moving parts, making them easier to secure and vent for vacuum environments. Switching to the smaller S-mount lens required reducing the pixel size. The Sony IMX547 sensor, with a pixel size of 2.74 µm, supports 5 MP resolution and allows the use of S-mount lenses. Additional advantages include a broader selection of focal lengths, particularly shorter ones, resulting in wider FOV.

2. Aperture & Focal Length Selection

The selection of the focal length and aperture heavily impacts navigation and perception capabilities. They are key parameters in determining the camera's FOV and hyperfocal distance. The FOV dictates how much of a scene in front of the camera is visible and affects near-sighted focusing. Since overlapping imagery from the stereo pair is used to calculate stereo disparity, a wider FOV results in increased frame overlap at nearer depths. Consequently, a wider FOV allows for the perception of depth of objects closer to the camera. However, it also increases depth error at greater distances in the scene.

Aperture selection impacts the camera's hyperfocal distance, which is the optimal focusing distance that provides the maximum depth of field, keeping as much of the scene as possible in focus and sharp. Generally, a shorter focal length and higher aperture f-number result in a shorter hyperfocal distance. A shorter hyperfocal distance is desirable because it improves image quality for close-up objects while maintaining sharpness throughout the scene. Conversely, a longer hyperfocal distance forces a compromise between the sharpness of nearer and farther objects. Additionally, aperture is a primary factor in camera exposure. A larger aperture (lower f-number) allows more light to reach the sensor. Given the harsh lunar lighting conditions with extreme contrast, it is important that the camera system is capable of high dynamic range and performs well in both very bright and dark scenes. An aperture of f/4 has shown positive results in a relevant test environment. It is critical that the aperture performs well in shadowed regions while not oversaturating the image sensor in bright conditions. While testing is ongoing to fine-tune these parameters, the selection has been considerably narrowed. Since it is critical for the excavator to perceive imminent hazards and collisions, the camera system must maintain high acuity at close range. Therefore, focal lengths of 6 mm and 4.4 mm are being evaluated with an aperture of f/4.

3. Baseline Selection

The baseline selection is a unique parameter constrained largely by the mechanical design of the overall IPEx system. Initial testing was conducted with individual cameras on opposite "shoulders" of the robot, with the arm system in between. This resulted in a large baseline of 16.5 cm (Fig. 28). However, this introduced a significant amount of material and structure between these two cameras. Since stereo disparity is highly sensitive to rigid mounting to maintain epipolar constraints, deflection and thermal expansion of the large structural chain between the cameras posed a risk to calibration (Fig. 29 and Fig. 30). While testing showed that this split design was functional and could be calibrated, a loss of stereo performance was noted. This risk, along with the poor performance of depth estimates at close range, led to the decision to combine the stereo pair cameras into a single housed unit. This design change improved rigidity, making stereo calibration more reliable and easier to maintain (Fig. 31 and Fig. 32). The reduced baseline, while increasing depth error at further distances, improves the accuracy of depth estimation of nearby objects which facilitates IPEx's ability to navigate its immediate environment effectively.

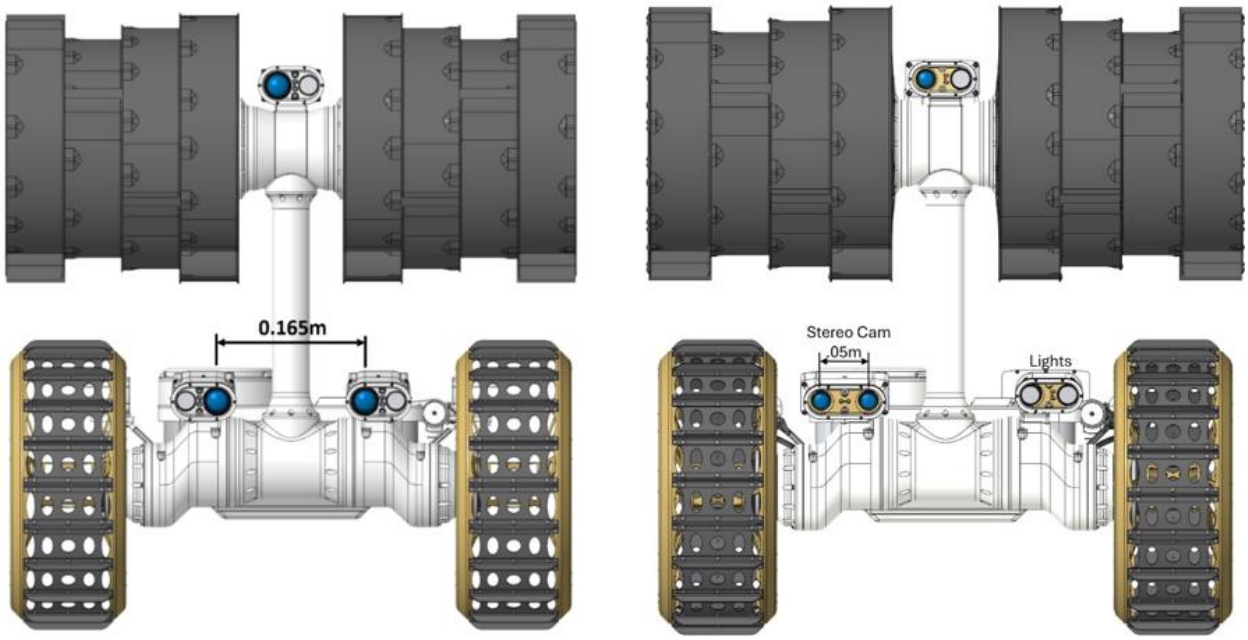

Fig. 28 Placement of camera pairs on IPEx with initial baseline (left) and reduced baseline (right).

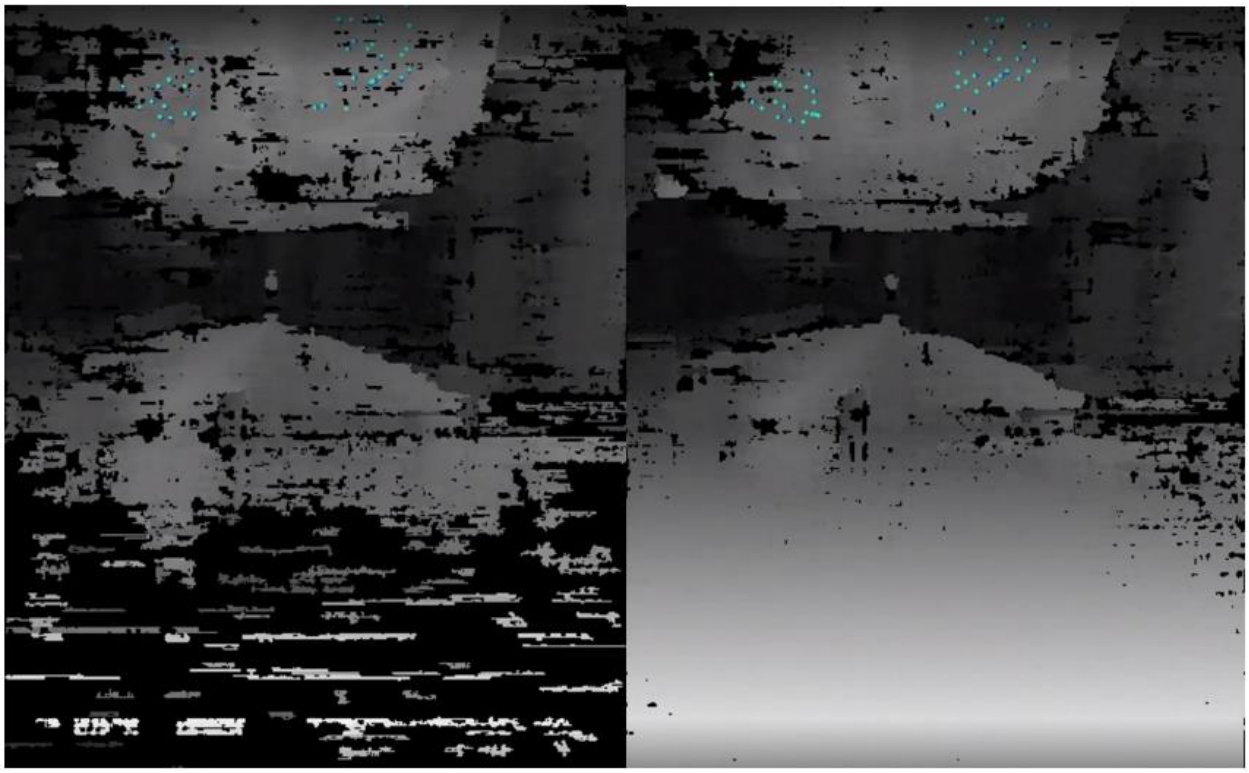

Fig. 29 Results of lost stereo calibration from an applied load with separated stereo camera units.

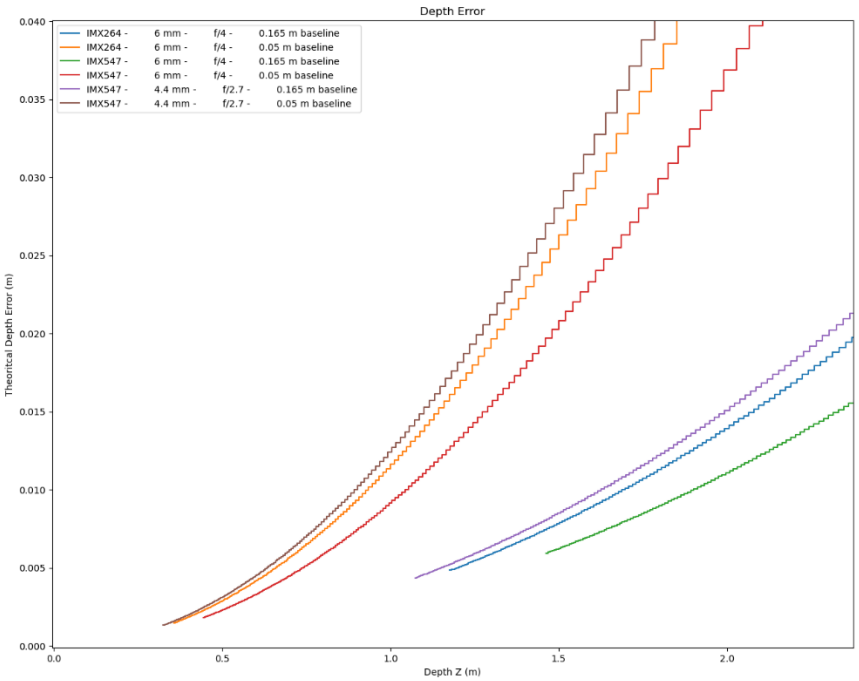

Fig. 30 Depth error and minimum depth capability of different stereo configurations.

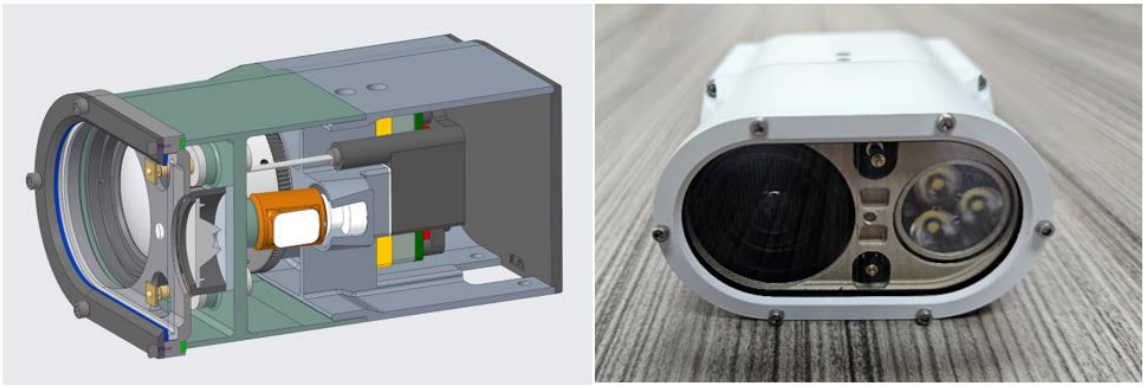

Fig. 31 Monocular camera module CAD (left) and as-built (right).

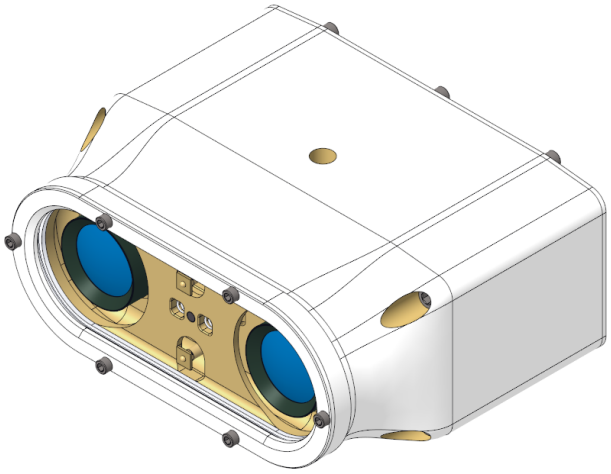

Fig. 32 Stereo camera CAD with reduced baseline.

4. Lighting Design

The lunar polar conditions present extreme challenges due to the high contrast, low sun angles, and the lack of atmosphere, making it difficult to image shadowed regions. To address this, LED illumination is integrated into the camera units. Each light can output a maximum of 3,000 lumens per light is possible and is focused by a total internal reflection (TIR) optic. The angle of the light output is approximately 42 ° (full width at half maximum). Each LED unit consists of three LEDs mounted to a circuit board. Each monocular camera has a single LED unit. The stereo camera modules do not have LED units, but there is a stereo LED unit mounted to the other side of the chassis. The stereo LED unit for the stereo pair consists of two LED units. In total, there are six LED units on IPEx.

B. Camera Dust Mitigation Design

Because IPEx's primary operation is to excavate and move regolith, it is expected to encounter significant amounts of dust that could obscure the cameras and prematurely end the mission. To mitigate this risk, IPEx employs a three-pronged approach. First, the cameras are outfitted with EDS lens covers. These transparent shields use alternating current to clear dust from the surface (Fig. 33). The EDS technology has been in development over the last decade and is manifested on upcoming CLPS missions to demonstrate its operation on the lunar surface [11]. Second, the EDS lens covers are attached to the camera modules using a HDRM that can jettison the lens cover if the EDS cannot clear the dust. While this contingency affords the mission additional time, the exposed lens will eventually become obscured beyond use. Finally, IPEx includes a fully redundant set of cameras to account for the unknown levels of dust loading that may be encountered.

Testing of the EDS system has verified that its dust-clearing performance is sufficient for continued operation. The requirement for this component allows for a portion of dust contaminants to remain after clearing. Tests were performed to verify that this residual dust does not occlude the vision systems. These tests involved "loading" the EDS glass in a lab setting with worst-case dust loads and then clearing the EDS. The glass was installed on a test rover system and driven in a relevant lighting environment to assess the performance of the vision and autonomy stack. With on-board illumination disabled, little affect was noted to image quality, and there was no significant impact to vision systems performance. However, with illumination enabled, some reflection was evident in the image due to the light being behind the same piece of EDS glass. This reflection caused visual artifacts and a loss of image quality that posed a risk to vision performance. For this reason, measures were taken to separate the light path from the camera system. For the stereo pairs, the lights were removed from the housing and installed on the opposite shoulder. This design change was logical since the stereo layout was being redesigned to improve the stereo camera baseline. For the monocular camera designs, additional material was installed to separate the illumination and camera sides of the housed unit. This additional material eliminated all glare at the camera.

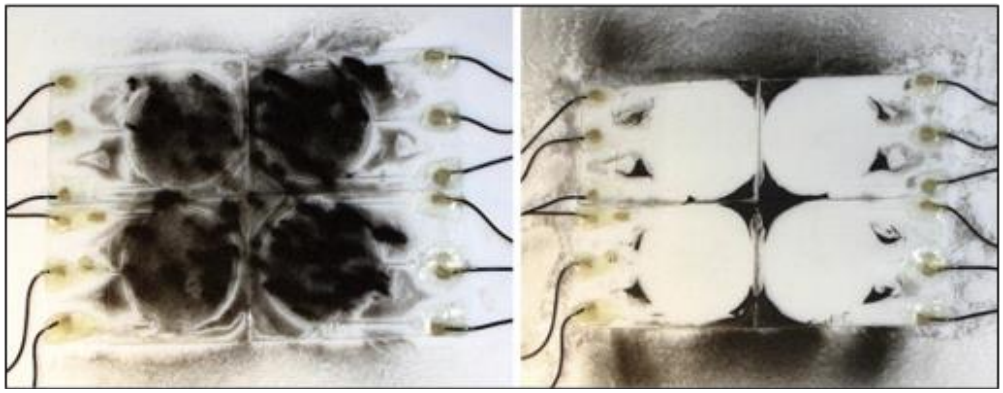

Fig. 33 EDS glass test clearing.

C. Camera and Dust Mitigation Testing

IPEx must be able to make decisions in-situ during its mission on the Moon. To achieve this, IPEx will use images obtained by eight on-board cameras to map the terrain surrounding it. To mitigate the risk of camera failure, the cameras functionality in different conditions is explored.

1. Imaging Distortion TVAC Test

At the Granular Mechanics and Regolith Operations (GMRO) Lab at KSC, the IPEx cameras underwent Thermal-Vacuum (TVAC) testing in the Atmospherically Sealed Simulator for In-situ System Testing (ASSIST) Vacuum

Chamber, and images were taken at different temperature steps to analyze any discrepancies that may have occurred due to temperature.

The two main camera calibration parameters that are affected by thermal gradients are the distortion coefficients and the camera matrix. The distortion coefficients account for radial distortion (caused by light bending more near the edges of the lens) and tangential distortion (caused by the sensor plane not being parallel to the lens). The camera matrix describes the focal lengths, optical center, and pixel skew. Changes in ambient temperature can cause thermal expansion of different parts of the camera; for example, any expansion in the lens will result in a change in radial distortion, whereas expansion in the camera housing can cause a change in both tangential distortion and the camera matrix. By characterizing these parameters changes over a range of temperatures, they can be accurately accounted for in the calibration process.

During testing of the IPEx cameras in the ASSIST Chamber, temperature control and data collection were performed using LabVIEW in conjunction with heaters and a cryogenic cold head ("cryohead"). Image capturing was performed manually for each temperature step using the FLIR SpinView software.

The temperature parameters used were based on the operational temperature range of the cameras, which was 0 to 50 °C, with added margin to push the performance limits. The vacuum level was maintained at 10^{-4} torr. There were five images captured for each step in the test matrix presented in Table 10.

Table 10 Test matrix for IPEx camera testing.

Step	Temperature (°C)
Take 5 photos per step	
0	0
1	5
2	10
3	15
4	20
5	25
6	30
7	35
8	40
9	45
10	50
11	Ambient (Vac)

The IPEx camera was interfaced onto the ASSIST Chamber with thermocouples and cartridge heaters, as well as copper straps and band clamps (Fig. 34). This created a thermally conductive path between the cryohead and the camera. MLI blankets were used to isolate the camera and copper straps. A calibration target was placed 22.9 cm from the front camera face and a paper blanket was placed around the MLI to prevent it from causing lighting inconsistencies on the target due to glare. Visual and software image comparisons were used to interpret the results qualitatively (Fig. 35).

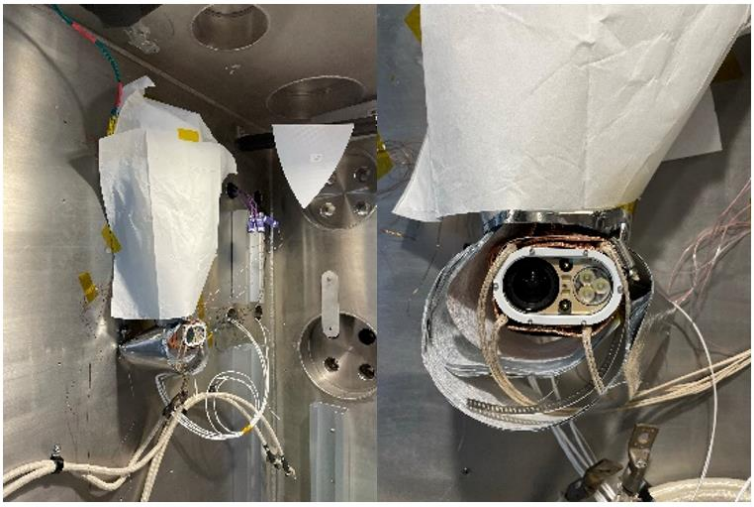

Fig. 34 IPEx camera installed in the ASSIST chamber.

Grey Hot Spot & Edge Blurring – During the first two iterations of the test, after turning the cryohead off, it was noted that a grey hot spot in the top right of the image and a grey blurring effect appeared around the edges of the camera. Most of the greying was concentrated at the right side of the image. It was concluded that the hot spot and edge blurring may have been due to residue or grease within the lens housing which surfaced once under vacuum.

Loss of Clarity – When heating the camera past operating temperature at 75 °C, the black areas of the image lost their clarity and became greyer. The greying appeared to be even across the image, aside from the hot spots and edge blurring as mentioned in the previous observation. After returning to room temperature, it was observed that the clarity was restored. It was concluded that the loss of clarity was related to operating the sensor outside of the recommended temperature range.

Image Shift – Software image comparison assessed the change in lens distortion using image subtraction by comparing pixel-shift from image to image. A 'bulging' effect was observed before and after pulling vacuum on the camera.

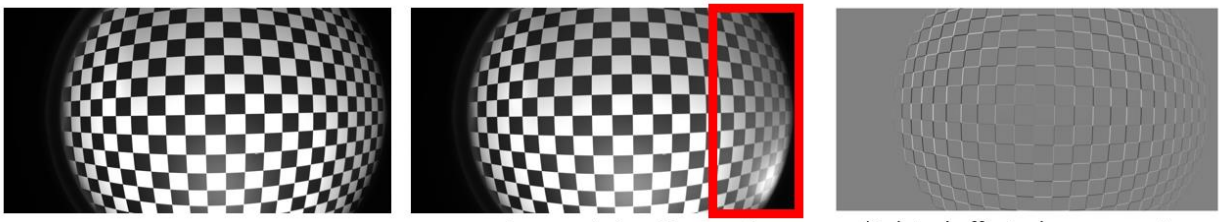

Fig. 35 ASSIST chamber camera views of calibration target.

From the ASSIST testing campaign, it was concluded that neither operation in vacuum nor at non-optimal temperatures caused permanent degradation to the sensor that caused concern for autonomy. However, the testing campaign raised concerns about off-gassing due to the lens choice and difficulties with baking out the cameras. This was a driving factor in the decision to switch the camera sensor to a variant that supports a smaller lens form factor. The new lens has a fixed aperture and is mechanically simpler, facilitating venting to address concerns with off-gassing and baking out the lens. This test campaign will be reconducted with the new camera sensor and lens.

2. Vibration & Shock Testing

The purpose of performing vibration and shock testing was to ensure that the COTS components can withstand GEVS qualification and Falcon 9 shock levels. This would give structural analysts confidence that the COTS glass components will survive with margin defined in NASA-STD-5001 and enable treatment of COTS components as

point masses in FEA. Furthermore, the vibration and shock testing would evaluate the structural support of the previous camera housing design to inform future iterations.

The testing consisted of one IDS camera sensor (GV-51F2SE Rev.4.2), one camera lens (low distortion 6mm M12), and one prototype camera assembly that included the previous camera housing design, the Glass EDS, the previous Kowa camera lens (LM6JC | 2/3" 6 mm MP C-mount lens), the previous FLIR sensor (BFS-GE-88S6M-BD2: 8.9 MP, 13 FPS, Sony IMX264, Monochromatic), and the EBAD HDRM (Fig. 36).

The testing sequence was as follows:

1) Random vibration testing to GEVS acceptance levels; all axes, 1 minute per axis
2) Random vibration testing to GEVS qualification levels; all axes, 1 minute per axis
3) Half-sine pulse testing to F9 shock loads (reference Table 4-9 in F9 PUG); all axes
4) Random vibration testing to 2x GEVS qualification levels; all axis, 10 seconds per axis
5) Random vibration testing to 3x GEVS qualification levels; all axes, 10 seconds per axis

For each test, the sensors were turned on to check for any dead pixels or irregularities before and after each test run. The glass on the lenses was visually inspected for breakage. It was concluded that the image quality for the IDS camera sensor and the FLIR camera sensor did not degrade from the vibration and shock testing. It was also noted that none of the glass features (glass EDS, camera lenses, glass on sensors) experienced any cracking from the testing.

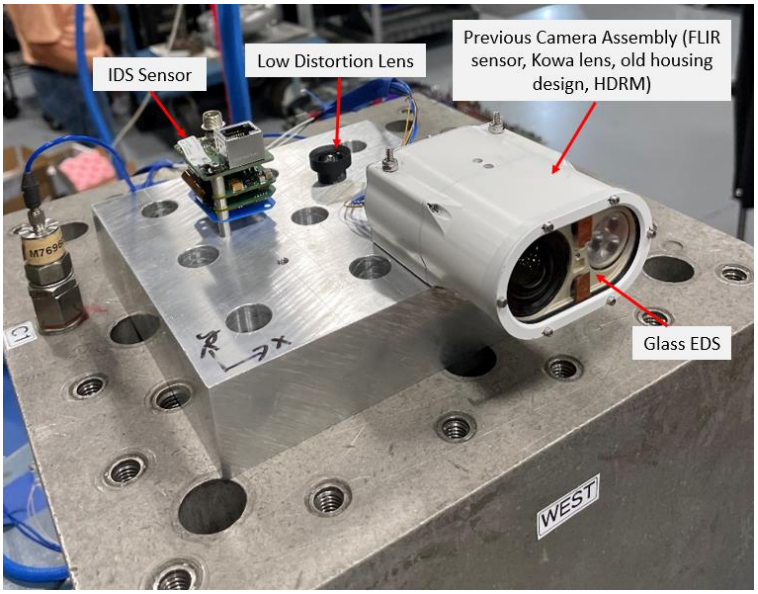

Fig. 36 Vibration and shock test setup.

3. HDRM Testing

The Camera HDRM utilizes Ensign-Bickford's Frangibolt technology in its launch locks. Frangibolt actuators operate by using a heating element to heat a shape memory alloy (SMA) cylinder, causing it to expand in length. The locked joint is preloaded through the SMA cylinder via a Titanium fastener. This fastener is notched radially at a specific point along its length: the separation joint plane. The increase in the SMA cylinder's length causes the Titanium fastener to snap at the notch, releasing the joint.

In the camera housing design, the Frangibolt secures the front frame of the camera to the rest of the housing (Fig. 37). When the HDRM is triggered, the Frangibolt snaps, causing springs within the housing to eject the front frame of the camera from the camera body, removing the glass EDS. The purpose of this feature is for if the glass EDS fails and the cameras lose visibility due to regolith build up on the glass, the HDRM would be activated to eject the glass and allow IPEx to run autonomously for a longer duration.

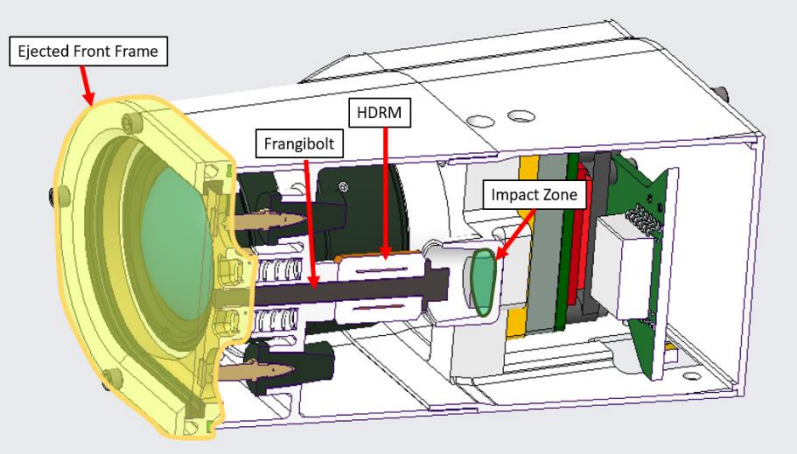

Fig. 37 Frangibolt and HDRM configuration in camera housing.

When the HDRM is triggered, the Frangibolt separates with momentum that translates into the housing body, causing shock to the components within the camera. The purpose of testing the HDRM is to observe if the camera internals (sensor, lens) still function after experiencing shock loads induced by actuating the HDRM.

From this test, it was found that the lens ejects approximately 15.2 cm away from the camera body in Earth's gravity (Fig. 38). Furthermore, the FLIR sensor continued to function, and there were no fractures or breakage observed in the camera body or the internal hardware. In a future iteration of this test, acceleration data will be obtained to characterize the induced shock from the Frangibolt.

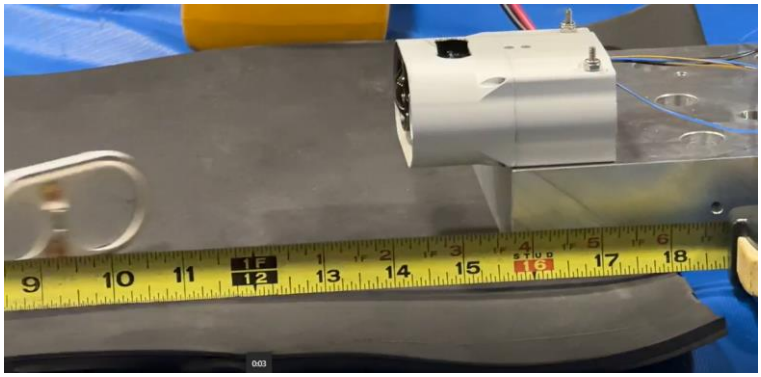

Fig. 38 Lens deploying from camera body after HDRM actuation.

VI. Thermal Control Subsystem

One of the major advancements from the RASSOR 2 (TRL-4) to IPEx TRL-5 is the thermal control system (Fig. 39). IPEx is designed to operate in the south pole region of the Moon and needs to reject the heat generated during its high operation rate. Traditionally, this would be done using a radiator panel to reject heat to space, however, IPEx will encounter significant amounts of dust that could cover a radiator and prevent it from functioning effectively. To address this, IPEx uses an actuated cover to protect its radiator. While the excavator is in operation, the radiator cover is closed to prevent dust from collecting on the sensitive surfaces. The heat generated during this mode is used to melt a phase change material (PCM). Once the PCM is fully melted, IPEx will pause operations and open the radiator cover, allowing the radiator to reject the stored heat energy to space and in-turn resolidifying the PCM. IPEx worked with a PCM vendor to fabricate a custom PCM heatsink, which is described in this section.

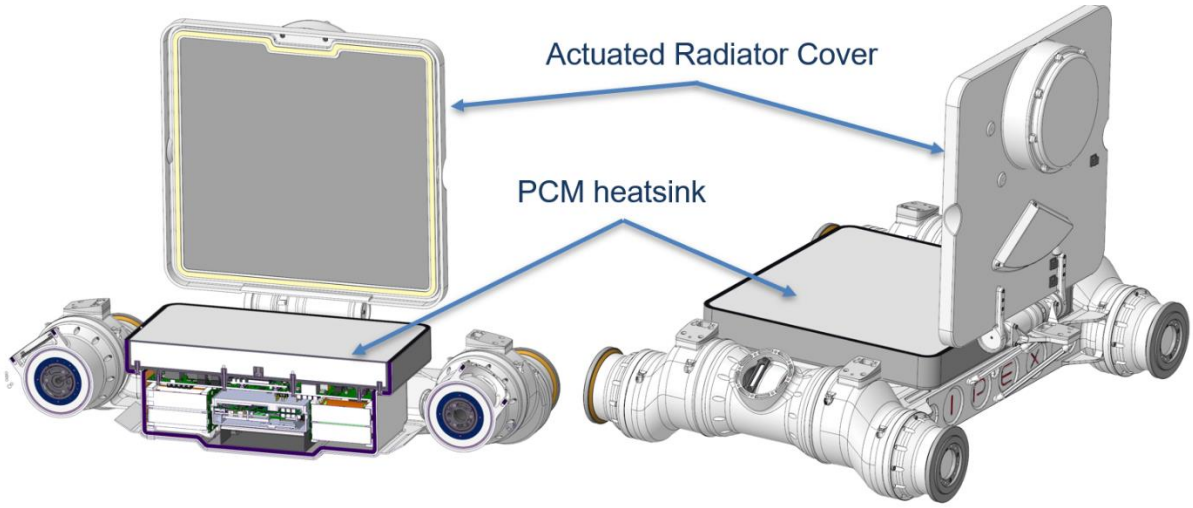

Fig. 39 Thermal Control System with radiator cover and PCM heatsink.

A. Radiator Cover Design and Testing

The radiator cover was designed to shield the radiator from dust and lift the wireless charger antenna for recharging operations. Additionally, the cover provides a rotational degree of freedom to help align the wireless charger during docking. The cover is constructed from polyetherimide (Ultem) due to its robustness and non-metallic properties, making it suitable for holding the wireless charger antenna. It is coated with Cerakote for added protection. A felt seal is seated under the cover to create a seal between the two surfaces when the cover is down. An MLI blanket under the cover acts as a thermal switch, preventing heat transfer to the PCM during operation (Fig. 40).

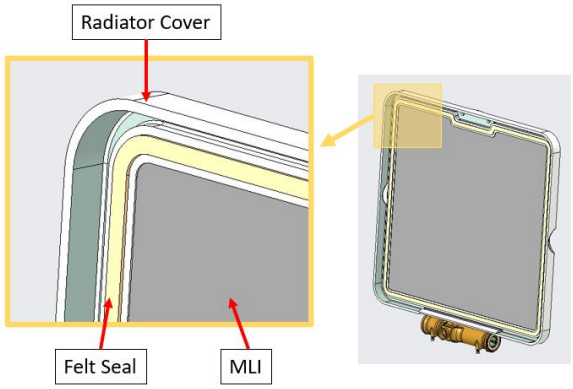

Fig. 40 Radiator cover assembly.

To validate that the radiator cover is an effective means of keeping regolith off the radiator, two areas were explored: the ballistic particle test and the radiator potential difference test.

1. Ballistic Particle Test

The purpose of the ballistic particle test was to determine how particles on top of the radiator cover would flow when the radiator cover actuates. The goal was to demonstrate that particles falling off the radiator cover due to actuation would not fall onto the radiator. This test served as an initial assessment to identify any major concerns with the radiator cover design that might cause large particles to fall onto the radiator.

The radiator cover was mounted to the chassis with the radiator cover motor, and silica sand was distributed evenly over it. Silica sand was selected as the simulant material since its round particles allowed for the focus to be strictly on ballistic behavior, eliminating lofting or cohesive properties. The radiator cover was moved 90° and footage was recorded to capture the flow. A sticky blue sheet was placed under the radiator cover to capture any possible stray particles (Fig. 41).

Fig. 41 Silica sand flowing off radiator cover during testing.

It was observed that there was minor accumulation of particles on the radiator cover motor and on the edge of the radiator closest to the motor (Fig. 42). The accumulation was attributed to particles falling from the cover and deflecting off the radiator cover motor onto the radiator itself. Future design of the radiator cover motor or radiator cover will consider this observation to mitigate regolith accumulating on the radiator due to the cover's actuation. Otherwise, there were no outstanding areas of particle accumulation, and the particles flowed as expected.

Fig. 42 Slight particle accumulation on radiator cover actuator and on edge of radiator

2. Radiator Potential Difference Test

When materials separate, there is potential for tribo-charging to occur that would create a potential difference around the radiator and the external environment. Since the radiator cover is separating from the radiator, there is concern that tribo-charging or other forms of charging from the configuration would create an electric field that could attract dust, given that the field would have different potentials from the fields where dust is co-located leading to a force that would loft the dust onto the radiator. In order to understand if this is a risk, characterization of tribo-charging between the radiator cover and radiator was necessary. This data would later inform the particle trajectory simulation study. The testing was conducted at the KSC Electro-Statics Physics Lab (ESPL).

For this test, the radiator was placed inside of a vacuum chamber and connected to a 100 pF capacitor to measure the peak voltage when the material was separated. An MLI blanket and Teflon sheet were used as the separating materials. Teflon was used to obtain a baseline surface charge on the radiator to compare to the surface charge caused by separation of the MLI blanket. Separation was performed by connecting the materials to a motor with a string that pulled the material off the radiator when powered on. Weights were added on top of the material to guarantee contact (Fig. 43).

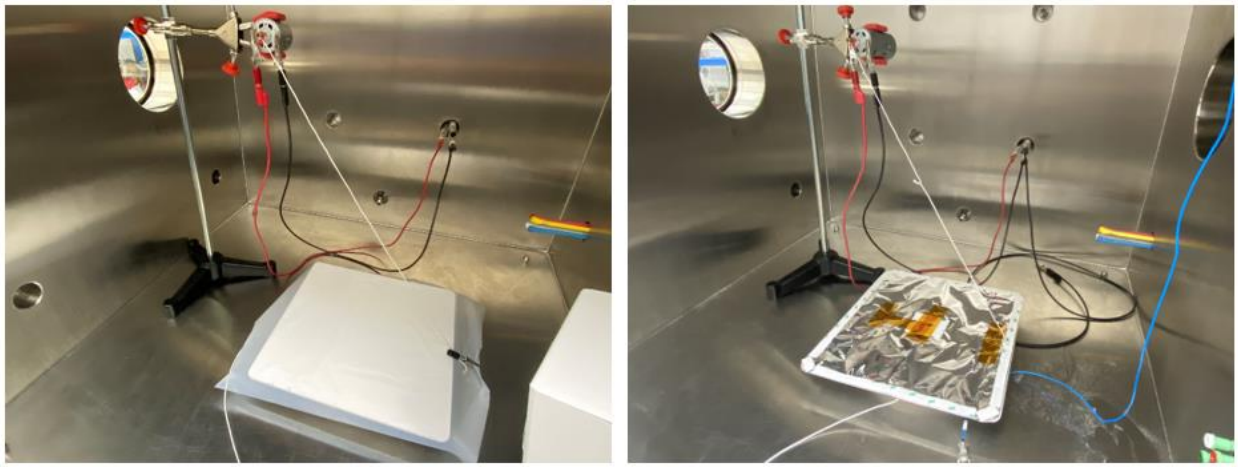

Fig. 43 Teflon (left) and MLI layer (right) on radiator cover.

Table 11 outlines the results of the tribo-charge test. Two surface charge densities were obtained and used in the particle trajectory simulation study.

Table 11 Results from tribo-charge experiment.

Condition	Capacitance (F)	Cap Voltage (V)	Charge (C)	Charge (nC)	Rubbed Material	Rubbing Material	Surface Charge Density (uC/m^2)
1E-5 Torr	1E-10	0.004	4E-13	0.0004	S13	MLI sheet	**5.25E-6**
1E-5 Torr	1E-10	0.006	6E-13	0.0006	S13	MLI sheet	**7.87E-6**

Using the results above, the surface charge density was compared to the surface charge density of the bucket drum arm was explored to determine whether the area around the arms would generate a stronger electric field than the field generated around the radiator. If this is the case, then the arms will be more likely to attract dust particles than the radiator. Calculations were performed by the ESPL to characterize the surface charge density of the bucket drum arm based on the mass of regolith (m) deposited on the arm. This data was used to inform a COMSOL particle trajectory model, as described in the following section.

The surface charge density of the bucket drum arm can be calculated by assuming a charge over mass (Q/m) of the particles. The ESPL used prior experimental Q/m data for regolith to directly calculate the surface charge density.

Given a particle diameter range, the constant Q/m, and the surface area of the drum arm (A), the surface charge density on the drum arm (σ) can be estimated:

$$Q = \frac{Q}{m} * m$$
$$\sigma = \frac{Q}{A} \quad (1)$$

Table 12 shows the calculated results from this study.

Table 12 Surface charge density on bucket drum arm.

Mass m (g)	Q/m (nC/g)	Q (nC)	Robotic arm surface area A (m^2)	Charge Density σ (uC/m^2)
0.01	-150	-1.5	0.013	**-1.15E-01**
0.05	-150	-7.5	0.013	**-5.77E-01**

0.1	-150	-15	0.013	**-1.15E+00**
0.2	-150	-30	0.013	**-2.31E+00**
0.3	-150	-45	0.013	**-3.46E+00**
0.4	-150	-60	0.013	**-4.62E+00**
0.5	-150	-75	0.013	**-5.77E+00**
0.6	-150	-90	0.013	**-6.92E+00**
0.7	-150	-105	0.013	**-8.08E+00**
0.8	-150	-120	0.013	**-9.23E+00**
0.9	-150	-135	0.013	**-1.04E+01**

When compared with the results from the tribo-charging test, the surface charge density on the bucket drum arm is expected to be higher. Therefore, the bucket drum arm is expected to generate a stronger electric field and is more likely to attract dust particles.

A COMSOL model was then used that included the radiator and the bucket drum arm with their corresponding charge densities (Fig. 44). The purpose of the model was to observe dust particle trajectory when in the presence of the radiator and the bucket drum arm. The simulation model was run for each of the values listed in Table 13 with the arm rotated at varying degrees to see how that would affect particles lofting onto the radiator.

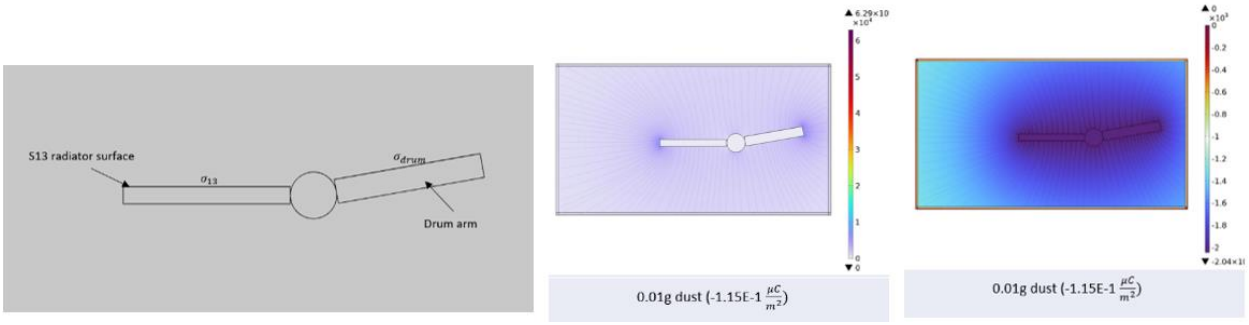

Fig. 44 COMSOL model setup (left), with electric field (middle), and voltage (right) plots.

Table 13 Particle trajectory model results.

Mass (g)	Charge Density (uC/m^2)	-10 degree	0 degree	10 degree	20 degree	30 degree	40 degree	50 degree	60 degree	70 degree	80 degree	90 degree
0.01	-1.15E-01											
0.05	-5.77E-01											
0.1	-1.15E+00											
0.2	-2.31E+00											
0.3	-3.46E+00											
0.4	-4.62E+00											
0.5	-5.77E+00											
0.6	-6.92E+00											
0.7	-8.08E+00											
0.8	-9.23E+00											
0.9	-1.04E+01											

Key: Green – No dust lofted, Yellow – dust lofted but not onto radiator, Red – dust lofted and onto radiator

From the results, it was observed that increasing the angle of the arm relative to the radiator would cause particles to land onto the radiator. Increase in particle count was observed to tolerate larger angles without lofting dust onto the radiator. It was concluded that when opening the radiator cover, the bucket drum arm should be positioned at 0° or lower to avoid dust lofting onto the radiator. This is shown in Fig. 45.

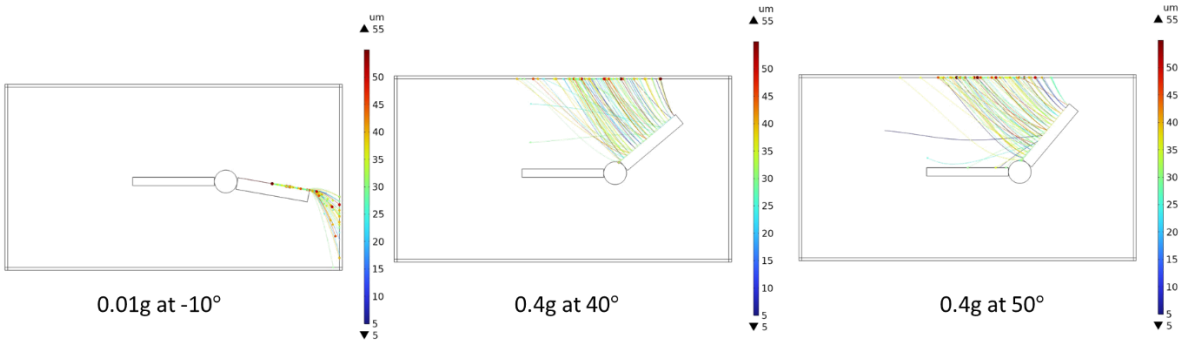

Fig. 45 Particle trajectory at varying bucket drum arm angles.

Overall, it was concluded that dust can loft onto the radiator due to electric fields produced by the surface charge on the radiator and bucket drum arm. Operational controls will be used to mitigate that effect. However further studies on static components around the radiator (radiator motor, cameras) will also need to be evaluated in the future.

B. Radiator Cover Actuator Selection

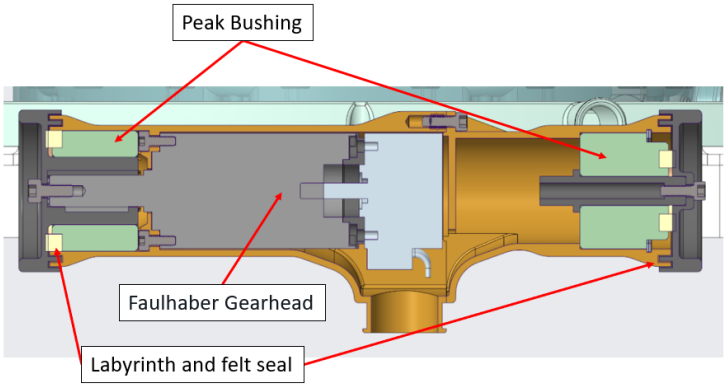

Fig. 46 Radiator cover actuator.

The radiator cover actuator (Fig. 46) raises and lowers the radiator cover for the thermal reset of the PCM and alignment of the wireless charger. The actuator was sized considering the worst-case load of raising the cover when regolith has settled on top of it. Estimating the amount of regolith loading during nominal operation is challenging due to difficulty of testing in relevant environments, such as dust in vacuum, low gravity, and lunar electrostatic effects. Therefore, an engineering bounding load case was used to account for potential inaccuracies in dust loading estimation. During nominal operation, the RDS arms do not rise above 55°, preventing the bucket drums from rising over the top of the radiator cover. However, in some contingency cases, the RDS arms may need to actuate so that the bucket drums are located above the radiator cover, potentially depositing regolith on top of the radiator cover. Using the self-facing camera and fiducial markers located on the radiator cover, the amount of regolith loading can be monitored throughout the mission.

If regolith loading is determined to exceed the radiator cover's peak torque capacity, one of the RDS arms can be lowered under the excavator to raise the chassis to about 45° allowing most of the regolith to slide off. It is assumed that the remaining regolith would be less than 3.2 mm thick. The leftover regolith is estimated to be 0.42 kg, assuming a density of 1.5 gram/cm^3. This results in a torque requirement of 1.84 N*m for peak operation.

The Faulhaber 2214X024BXTH + 22GPT 862:1 was selected for the radiator cover actuator. The gearhead has a continuous output torque of 1.8 N*m and a peak torque of 2.5 N*m. The opening time of the radiator cover was determined to be 30 seconds to reduce the dynamic nature of failing regolith from the cover, resulting in a motor speed of 431 RPM. The Faulhaber gearhead can be ordered vacuum-rated with vacuum grease preinstalled. The Hall effect sensor part number could not be identified, so further qualification is required. Future testing of the radiator cover motor will follow the same methodology as described in section IV, Actuator Test Campaign earlier in the paper.

C. Phase Change Material Design

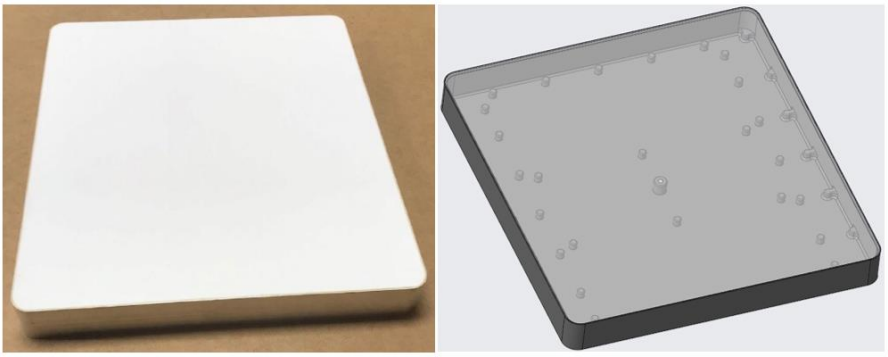

Fig. 47 PCM hardware on left, PCM cavity shown with transparent radiator plate on right.

The PCM housing is made from 6061 aluminum and features an internal cavity sized to retain the PCM (Fig. 47). The bottom of the PCM housing serves as the conductive interface to the avionics enclosure. The cavity is filled with aluminum fins bonded inside using thermal epoxy. The fins help distribute the heat load throughout the PCM and transfer heat from the bottom to the top as the PCM expands and contracts due to temperature variations.

The cover, also made from 6061 aluminum, doubles as the radiator surface and is glued into place after the fins are inserted. A port at the bottom of the cavity allows for filling the PCM after the assembly. The cover is coated with S13GLO thermal paint, a low outgassing version white thermal paint made with zinc oxide pigment in an RTV602 silicone binder. The calculated latent heat capacity of the PCM is 300.5 kJ. The phase change material is n-Hexadecane 99+%, which has a melting temperature of 18 °C.

The PCM assembly weighs 2.5 kg. A transient thermal analysis was completed using Thermal Desktop software to model the thermal behavior of IPEx throughout the mission. This model sized the required latent heat capacity needed. The PCM housing was designed at KSC, while the internal design, including fins and PCM filling, was completed at KULR. KULR also defined the required internal volume to achieve the required latent heat capacity. Vacuum chamber testing of the PCM assembly is planned to ensure even heat transfer throughout the PCM from the avionics. This test will address the time-varying non-uniform heat load of the avionics.

VII. Conclusion

This paper has reviewed the design and testing of the primary subsystems for the TRL-5 IPEx, including the Mobility Subsystem, Regolith Delivery Subsystem, Camera and Dust Mitigation Subsystem, and Thermal Control Subsystem. It is the authors' goal to disseminate as much information as possible about the development of this unique robotic excavator to help enable a sustainable future of Lunar and Martian exploration. The IPEx team will continue to publish and communicate detailed updates on the progress of this technology development. A public website has been established that will serve as a hub for IPEx-related information and can be found at https://www.nasa.gov/isru-pilot-excavator/.

Acknowledgments

The authors would like to thank the NASA Space Technology Mission Directorate and the Game Changing Development program which funds the IPEx project. Additionally, we would like to acknowledge the contributions of our IPEx team members from the Jet Propulsion Laboratory on the design and analysis of the thermal control system.

References

[1] Sanders, G. B., "Advancing In-Situ Resource Utilization Capabilities to Achieve a New Paradigm in Space Exploration," *AIAA SPACE and Astronautics Forum and Exposition*, p. 5124, 2018. DOI: 10.2514/6.2018-5124.

[2] Heiken, G., Vaniman, D., and French, B. M., "Lunar Sourcebook: A User's Guide to the Moon," *Cambridge University Press*, 1991. https://ntrs.nasa.gov/citations/19920057201

[3] Sanders, G. B., Larson, W. E., Sacksteder, K. R., Mclemore, C., and Johnson, K., "NASA In-Situ Resource Utilization (ISRU) Technology and Development Project Overview," *Space Technology Applications International Forum*, presentation, 2008. https://ntrs.nasa.gov/citations/20080010672

[4] Mueller, R. P., Smith, J. D., Schuler, J. M., Nick, A. J., Gelino, N. J., Leucht, K. W., Townsend, I. I., and Dokos, A. G., "Design of an Excavation Robot: Regolith Advanced Surface Systems Operations Robot (RASSOR) 2.0," *ASCE Earth and Space*, pp. 163-174, 2016. DOI: 10.1061/9780784479971.018.

[5] Kimmel, W. M., Beauchamp, P. M., Frerking, M. A., Kline, T. R., Vassigh, K. K., Willard, D. E., Johnson, M. A., Trenkle, T. G., "Technology Readiness Assessment: Best Practices Guide," *NASA Special Publication*, 2020. https://ntrs.nasa.gov/citations/20205003605

[6] Clark, C., Smith, J. D., Nick, A., Ortega, V., Kennett, A., Dillon, R. P, and Buckles, B., "Experimental Capabilities and Achievements of the Space Environment Dynamometer (SED)," *IEEE Aerospace Conference*, 2023. DOI: 10.1109/AERO055745.2023.10115922.

[7] Cao, C., Rogg, A., and Tardy, A., "Actuated Suspension Tuning Characterization of the VIPER Lunar Rover," *IEEE Aerospace Conference*, pp. 1-11, 2023. DOI: 10.1109/AERO55745.2023.10115796.

[8] Zhang, L., Schuler, J., Dokos, A., Xu, Y., Bell, E., and Muller, T. "ISRU Pilot Excavator Wheel Testing in Lunar Regolith Simulant," *ASCE Earth and Space, to appear*, 2024. https://ntrs.nasa.gov/citations/20240001016

[9] Buckles, B. C., Schuler, J. M., Nick, A. J., Smith, J. D., Muller, T. J., "ISRU Pilot Excavator - Development of Autonomous Excavation Algorithms," *Space Resources Roundtable, XXII Meeting*, 2022. https://ntrs.nasa.gov/citations/20220005125

[10] Schuler, J., Nick, A., Leucht, K., Langton, A., and Smith, D., "ISRU Pilot Excavator: Bucket Drum Scaling Experimental Results," *ASCE Earth and Space*, pp. 394-407, 2022. DOI: 10.1061/9780784484470.037.

[11] Calle, C. I., Immer, C. D., Clements, J. S., Chen, A., Buhler, C. R., Lundeen, P., Mantovani, J. G., Starnes, J. W., Michalenko, M., and Mazumder, M. K., "Electrodynamic dust shield for surface exploration activities on the Moon and Mars," *International Astronautical Congress Conference*, 2006. DOI: 10.2514/6.IAC-06-A5.2.07.